Electronic Supplementary Material (ESI) for Dalton Transactions.
This journal is © The Royal Society of Chemistry 2023

Supporting Information

θ-$[Mo_8O_{26}]^{4-}$-Based Hybrid Material for High Catalytic Performance on Cycloaddition of CO_2, Esterification and Knoevenagel Condensation

Zhengguo Zhang,[a] Hongxiao Lv,[c] Kun Yang,*[,b] Xiutang Zhang[c,]*

[a]Department of Materials Science and Engineering，Shanxi Institute of Technology，Yangquan, 045000, People's Republic of China. [b]Teachers College, Inner Mongolia University of Science and Technology, Baotou 014030, China

[c]School of Ehemistry and Chemical Engineering, North University of China, Taiyuan 030051, People's Republic of China.

Contents

Experimental Section

Table S1. Crystallographic data and refinement parameters of **NUC-62**.

Table S2. Selected bond lengths and angles of **NUC-62**.

Table S3. The hydrogen bond of **NUC-62**.

Table S4. Comparison of the catalytic activity of various POMs for the cycloaddition of CO_2 with epoxides.

Table S5. Comparison of the catalytic activity of various POMs for the knoevenagel condensation reaction.

Table S6. Comparison of the catalytic activity of various POMs for the esterification condensation reaction.

Figure S1. The $Co_2(BPPP)_2(C_2O_4)_2$ fragment, $[Mo_6O_{19}]$ cluster and the open network of $[Co_2(BPPP)_2(C_2O_4)_2][Mo_6O_{19}]$.

Figure S2. The $[Ni(BPPP)]_2$ fragment, $[Mo_8O_{26}]$ cluster and the open network of $[Ni(BPPP)]_2\{\varepsilon\text{-}[Mo_8O_{26}]\}$.

Figure S3. The $[Zn(BPPP)]_2$ fragment, $[Mo_8O_{26}]$ cluster and the open network of $[Zn(BPPP)]_2\{\beta\text{-}[Mo_8O_{26}]\}$.

Figure S4. The $[Cd_2(BPPP)_2Cl_2]$ fragment, $[Mo_6O_{19}]$ cluster and the open network of $[Cd_2(BPPP)_2Cl_2][Mo_6O_{19}]$.

Figure S5. The PXRD patterns of as-synthesized **NUC-62** and simulated.

Figure S6. The FT-IR spectrum of as-synthesized **NUC-62**.

Figure S7. ^{1}H NMR spectrum of 4-fluoro-1,3-dioxolan-2-one.

Figure S8. ^{1}H NMR spectrum of 4-chloro-1,3-dioxolan-2-one.

Figure S9. ^{1}H NMR spectrum of 4-methyl-1,3-dioxolan-2-one.

Figure S10. ^{1}H NMR spectrum of 4-(trifluoromethyl)-1,3-dioxolan-2-one.

Figure S11. ^{1}H NMR spectrum of 4-ethyl-1,3-dioxolan-2-one.

Figure S12. ^{1}H NMR spectrum of 4-ethenyl-1,3-dioxolan-2-one.

Figure S13. ^{1}H NMR spectrum of 4-benzyl-1,3-dioxolan-2-one.

Figure S14. Recyclability study (five cycles) for catalytic activities of **NUC-62** in cycloaddition reaction.

Figure S15. The PXRD patterns of **NUC-62** and used **NUC-62** after fifth cycloaddition reactions.

Figure S16. The FT-IR patterns of **NUC-62** and used **NUC-62** after fifth cycloaddition reactions.

Figure S17. Evidence of heterogeneous nature of **NUC-62** in the cycloaddition reaction.

Figure S18. ^{1}H NMR spectrum of methyl benzoate.

Figure S19. ^{1}H NMR spectrum of methyl 4-fluorobenzoate.

Figure S20. ^{1}H NMR spectrum of methyl 4-chlorobenzoate.

Figure S21. ^{1}H NMR spectrum of methyl 4-bromobenzoate.

Figure S22. ^{1}H NMR spectrum of methyl 4-nitrobenzoate.

Figure S23. ^{1}H NMR spectrum of methyl 4-hydroxybenzoate.

Figure S24. ^{1}H NMR spectrum of methyl 4-methylbenzoate.

Figure S25. ^{1}H NMR spectrum of methyl 2,4-dimethylbenzoate.

Figure S26. ^{1}H NMR spectrum of methyl 3,5-dimethylbenzoate.

Figure S27. ^{1}H NMR spectrum methyl 2,4,6-trimethylbenzoate.

Figure S28. Recyclability study (five cycles) for catalytic activities of **NUC-62** in esterification condensation reaction.

Figure S29. The PXRD patterns of **NUC-62** and used **NUC-62** after fifth esterification condensation reaction.

Figure S30. The FT-IR patterns of **NUC-62** and used **NUC-62** after fifth esterification condensation reaction.

Figure S31. Evidence of heterogeneous nature of **NUC-62** in the esterification condensation reaction.

Figure S32. ^{1}H NMR spectrum of 2-(phenylmethylidene)propanedinitrile.

Figure S33. ^{1}H NMR spectrum of 2-[(4-fluorophenyl)methylidene]propanedinitrile.

Figure S34. ^{1}H NMR spectrum of 2-[(4-chlorophenyl)methylidene]propanedinitrile.

Figure S35. ^{1}H NMR spectrum of 2-[(4-nitrophenyl)methylidene]propanedinitrile.

Figure S36. ^{1}H NMR spectrum of 2-[(3,4-dimethoxyphenyl)methylidene]propanedinitrile.

Figure S37. ^{1}H NMR spectrum of 2-[(3,4,5-trimethoxyphenyl)methylidene]propanedinitrile.

Figure S38. ^{1}H NMR spectrum of 2-[(4-methylphenyl)methylidene]propanedinitrile.

Figure S39. ^{1}H NMR spectrum of 2-[(3,4-dimethylphenyl)methylidene]propanedinitrile.

Figure S40. ^{1}H NMR spectrum of methyl 4-[4-(2,2-dicyanoeth-1-en-1-yl)phenoxy]benzoate.

Figure S41. Recyclability study (five cycles) for catalytic activities of **NUC-62** in knoevenagel condensation reaction.

Figure S42. The PXRD patterns of **NUC-62** and used **NUC-62** after fifth knoevenagel condensation reaction.

Figure S43. The FT-IR patterns of **NUC-62** and used **NUC-62** after fifth knoevenagel condensation reaction.

Figure S44. Evidence of heterogeneous nature of **NUC-62** in the knoevenagel condensation reaction.

Experimental Section

X-ray crystallography. A summary of crystallographic data, refinement parameter and bond lengths and angles for **NUC-62** were given in Table S1 and S2. The diffraction intensity data for **NUC-62** was obtained at 298(2) K by using a Bruker Smart-APEX II CTM area detector (Mo-Kα radiation, λ=0.071073 nm) with graphite-monochromated radiation. The data integration and reduction were processed with SAINT software. The reflection data were consequently corrected for empirical absorption corrections and Lorentz and polarization effects. The structure was solved by direct methods and refined by full-matrix least-squares with the SHELXL package. All non-hydrogen atoms were refined anisotropically, until convergence was attained. Hydrogen atoms except those on water molecules were generated geometrically with fixed isotropic thermal parameters, and included in the structure factor calculations. The block of SQUEEZE in PLATON was employed to eliminate the highly disordered solvent molecular. Further details on the crystal structure investigations may be obtained from the Cambridge Crystallographic Data Centre, with the depository number CCDC-2219767 for **NUC-62**.

Table S1. Crystallographic data and refinement parameters of **NUC-62-NUC-66**.

Complex	**NUC-62**	**NUC-63**	**NUC-64**	**NUC-65**	**NUC-66**
Formula	$C_{38}H_{36}Cu_2Mo_4N_{12}O_{13}$	$C_{40}H_{36}Co_2Mo_6N_{12}O_{23}$	$C_{38}H_{36}Mo_8N_{12}Ni_2O_{26}$	$C_{38}H_{36}Mo_8N_{12}O_{26}Zn_2$	$C_{38}H_{40}Cd_2Mo_8N_{12}O_{28}$
Mr	1379.63	1746.31	1961.73	1975.05	2105.14
Crystal system	triclinic	triclinic	triclinic	monoclinic	triclinic
Space group	P-1(2)	P-1	P-1	$P2_1/n$	P-1
a (Å)	11.3387(13)	9.320(4)	9.572(12)	12.139(16)	10.666(19)
b (Å)	14.7820(17)	10.635(4)	11.799(14)	17.994(2)	12.257(2)
c (Å)	16.0037(19)	14.159(5)	13.565(2)	12.736(17)	13.960(4)
α (°)	115.799	92.791(4)	93.887(2)	90	105.246(2)
β (°)	99.611	96.522(4)	110.551(10)	93.862(10)	110.232(2)
γ (°)	92.807	93.237(3)	99.843(10)	90	104.322(2)
V(Å^3)	2358.64(50)	1390.0(9)	1399.8(3)	2775.6(6)	1528.5(6)
Z	2	1	1	2	1
Dcalcd(g·cm^{-3})	1.943	2.086	2.327	2.363	2.287
μ(mm^{-1})	1.991	1.977	2.478	2.685	2.353
GOF	1.038	0.966	0.997	1.046	0.999
R_1 [I>2σ(I)]a	0.0297	0.0502	0.0244	0.0238	0.0320
wR_2 [I>2σ(I)]b	0.0618	0.1039	0.0705	0.0590	0.1001
R_1a (all data)	0.0429	0.1015	0.0300	0.0301	0.0371
wR_2b (all data)	0.0663	0.1247	0.0741	0.0619	0.1044
R_{int}	0.0236	0.0458	0.0183	0.0440	0.0182

$^aR_1=\sum\big|\,|F_o|-|F_c|\,\big|/\sum|Fo|$. $^bwR_2=\big|\sum w(|F_o|^2-|F_c|^2)\big|/\sum\big|w(F_o^2)^2\big|^{1/2}$

Table S2. Selected bond lengths and angles of **NUC-62**.

Selected bond lengths (Å)			
Cu(1) -N(1)	2.052(4)	Cu(1) -N(2)	2.034(4)
Cu(1) -N(7)	2.082(4)	Cu(1) -N(8)	1.994(3)
Cu(2) -N(5)	2.055(3)	Cu(2) -N(6)	2.062(3)
Cu(2) -N(11)	2.018(3)	Cu(2) -N(12)	2.082(3)
Mo(3)-O(2)	2.335(2)	Mo(3)-O(4)#1	2.413(2)
Mo(3)-O(5)#1	1.919(2)	Mo(3)-O(8)	1.680(3)
Mo(3)-O(9)	1.682(2)	Mo(3)-O(10)	1.953(2)
Mo(1)-O(1)	1.767(2)	Mo(1)-O(2)	1.765(2)
Mo(1)-O(3)	1.699(2)	Mo(1)-O(4)	1.794(2)
Mo(4)-O(10)	1.843(3)	Mo(4)-O(11)	1.692(3)
Mo(4)-O(12)	1.693(3)	Mo(4)-O(13)	1.844(2)
Mo(2)-O(1)#1	2.355(2)	Mo(2)-O(4)	2.331(2)
Mo(2)-O(5)	1.892(2)	Mo(2)-O(6)	1.696(2)
Mo(2)-O(7)	1.688(2)	Mo(2)-O(13)	1.964(2)
Selected angles (°)			
N(1) -Cu(1)-N(7)	131.69(15)	N(2) -Cu(1)-N(1)	79.99(16)
N(2) -Cu(1)-N(7)	114.78(14)	N(8) -Cu(1)-N(1)	123.75(15)
N(8) -Cu(1)-N(2)	133.98(14)	N(8) -Cu(1)-N(7)	80.20(13)
N(5) -Cu(2)-N(6)	80.52(12)	N(5) -Cu(2)-N(12)	111.81(12)
N(6) -Cu(2)-N(12)	139.78(12)	N(11) -Cu(2)-N(5)	133.86(12)
N(11) -Cu(2)-N(6)	120.04(12)	N(11) -Cu(2)-N(12)	78.98(12)
O(2) -Mo(3)-O(4)#1	73.90(10)	O(5) #1 -Mo(3)-O(2)	80.43(9)
O(5) #1 -Mo(3)-O(4)#1	71.40(9)	O(5) #1 -Mo(3)-O(10)	147.21(10)
O(8) -Mo(3)-O(2)	163.53(12)	O(8) -Mo(3)-O(4)#1	90.37(12)
O(8) -Mo(3)-O(5)#1	99.46(11)	O(8) -Mo(3)-O(9)	105.33(14)
O(8) -Mo(3)-O(10)	97.41(12)	O(9) -Mo(3)-O(2)	90.85(12)
O(9) -Mo(3)-O(4)#1	163.23(12)	O(9) -Mo(3)-O(5)#1	99.66(11)
O(9) -Mo(3)-O(10)	102.69(12)	O(10) -Mo(3)-O(2)	75.58(10)
O(10) -Mo(3)-O(4)#1	80.61(9)	O(1) -Mo(1)-O(4)	109.61 (13)
O(2) -Mo(1)-O(1)	110.09(11)	O(2) -Mo(1)-O(4)	111.42(12)
O(3) -Mo(1)-O(1)	108.59(13)	O(3) -Mo(1)-O(2)	107.04(13)
O(3) -Mo(1)-O(4)	110.02(14)	O(10) -Mo(4)-O(13)	127.91(11)
O(11) -Mo(4)-O(10)	104.27(12)	O(11) -Mo(4)-O(12)	106.41(18)
O(11) -Mo(4)-O(13)	106.21(12)	O(12) -Mo(4)-O(10)	106.71(15)
O(12) -Mo(4)-O(13)	103.81(13)	O(4) -Mo(2)-O(1)#1	75.20(10)
O(5) -Mo(2)-O(1)#1	80.79(9)	O(5) -Mo(2)-O(4)	73.80(9)
O(5) -Mo(2)-O(13)	149.04(10)	O(6) -Mo(2)-O(1)#1	89.72(11)
O(6) -Mo(2)-O(4)	164.37(12)	O(6) -Mo(2)-O(5)	100.13(11)
O(6) -Mo(2)-O(13)	99.63(11)	O(7) -Mo(2)-O(1) #1	164.55(12)
O(7) -Mo(2)-O(4)	90.92(12)	O(7) -Mo(2)-O(5)	102.15(11)

O(7) -Mo(2)-O(6)	104.52(13)	O(7) -Mo(2)-O(13)	95.67(11)
O(13) -Mo(2)-O(1) #1	75.71(9)	O(13) -Mo(2)-O(4)	80.86(9)
Symmetry transformations used to generate equivalent atoms: [1]-x,-y,-z+1;			

Table S3. The hydrogen bond of **NUC-62**.

C---H···O	Hydrogen Bond distance
C(7)---H(7)···O(7)	2.34
C(9)---H(9A)···O(6)	2.56
C(10)---H(10A)···O(11)	2.56
C(12)---H(12)···O(11)	2.47
C(27)---H(27)···O(6)	2.38
C(29)---H(29A)···O(6)	2.53
C(36)---H(36)···O(8)	2.48
C(37)---H(37)···O(12)	2.55

Table S4. Comparison of the catalytic activity of various POMs for the cycloaddition of CO_2 with epoxides.

Catalyst	Catalyst dosage	TBAB dosage	Temperature (℃)	Pressure (atm)	Time (h)	Yield (%)	Ref.
$[Co_{2.5}(LOH)(LO)_2(H_2O)_2(PW_{12}O_{39})]\cdot 3CH_3CN\cdot 2OH$	10mg	0.16g	60	1	4	97	S1
$(NH_4)_4[ZnMo_6O_{18}(C_4H_8NO_3)(OH)_3]\cdot 4H_2O$	20mmol	0.15 mol%	70	1	3	99	S2
$[Mn(CO)_3]^+$	0.23 mol%	-	70	1.5	1.5	96	S3
$NaSiNb_{12}$	0.1g	-	120	1	10	96.5	S4
POMs	2 mol%	2.5 mol%	80	1	12	> 99	S5
$[Cu_2(BPPP)_2]\{\theta\text{-}[Mo_8O_{26}]\}$	0.18 mol%	0.5 mol%	65	1	6	92	This work

References:

S1. Zhao, Y. Q., Liu, Y. Y., & Ma, J. F. Polyoxometalate-Based Organic–Inorganic Hybrids as Heterogeneous Catalysts for Cycloaddition of CO_2 with Epoxides and Oxidative Desulfurization Reactions. *Crystal Growth & Design*, 2020, *21*, 1019-1027.

S2. Yu, W. D., Zhang, Y., Han, Y. Y., Li, B., Shao, S., Zhang, L. P., & Yan, J. Microwave-assisted synthesis of tris-Anderson polyoxometalates for facile CO_2 cycloaddition. *Inorganic Chemistry*, 2021, *60*, 3980-3987.

S3. Jia, J., Niu, Y., Zhang, P., Zhang, D., Ma, P., Zhang, C., & Wang, J. A Monomeric Tricobalt (II)-Substituted Dawson-Type Polyoxometalate Decorated by a Metal Carbonyl Group: $[P_2W_{15}O_{56}Co_3(H_2O)_3(OH)_3Mn(CO)_3]^{8-}$. *Inorganic Chemistry*, 2017, *56*, 10131-10134.

S4. Ge, W., Wang, X., Zhang, L., Du, L., Zhou, Y., & Wang, J. Fully-occupied Keggin type polyoxometalate as solid base for catalyzing CO_2 cycloaddition and Knoevenagel condensation. *Catalysis Science & Technology*, 2016, *6*, 460-467.

S5. Cheng, W., Xue, Y. S., Luo, X. M., & Xu, Y. A rare three-dimensional POM-based inorganic metal polymer bonded by CO_2 with high catalytic performance for CO_2 cycloaddition. *Chemical Communications*, 2018, *54*, 12808-12811.

Table S5. Comparison of the catalytic activity of various POMs for the Knoevenagel Condensation reaction.

Catalyst	Catalyst dosage	Solvent	Temperature (°C)	Time (h)	Yield (%)	Ref.
$NaSiNb_{12}$	0.05g	Methanol	25	2	99.8	S4
POVCOF 1	0.1	-	rt	0.5	99	S6
$[H_4Ta_6O_{19}]^{4-}$	10 μmol	DMSO	-	24	83	S7
$P_2W_{18}O_{68}$	0.010g	H_2O	rt	1	90	S8
Na-A-PW9	0.25 mol%	MeOH	rt	6	92	S9
Fe_3O_4@SiO_2@NH-NH_2-PW	0.040g	H_2O	Reflux	0.2	93	S10
PMOF3	0.2 mol%	Acetonitrile	45	1	>98.5	S11
$[H_2N(CH_3)_2]_2Na_{18}Cs_2H_{13}[(Cs_7(H_2O)_6)$@$\{(PO_4)$@$(Ni_4(OH)_3(WO_4))_3$@$(B\text{-}\alpha\text{-}PW_9O_{34})_3\}_2]\cdot 30H_2O$	1 mol%	Methanol	30	0.5	99	S12
$[Cu_2(BPPP)_2]\{\theta\text{-}[Mo_8O_{26}]\}$	0.16 mol%	Methanol	64.8	6	97	This work

References:

S6. Dou, M. Y., Zhong, D. D., Huang, X. Q., & Yang, G. Y. Imidazole-induced self-assembly of polyoxovanadate cluster organic framework for efficient Knoevenagel condensation under mild conditions. *CrystEngComm*, 2020, *22*, 4147-4153.

S7. Hayashi, S., Sasaki, N., Yamazoe, S., & Tsukuda, T. Superior base catalysis of group 5 hexametalates $[M_6O_{19}]^{8-}$ (M= Ta, Nb) over group 6 hexametalates $[M_6O_{19}]^{2-}$ (M= Mo, W). *The Journal of Physical Chemistry C*, 2018, *122*, 29398-29404.

S8. Khoshnavazi, R., Bahrami, L., & Rezaei, M. Heteropolytungstostannate as a homo-and heterogeneous catalyst for Knoevenagel condensations, selective oxidation of sulfides and oxidative amination of aldehydes. *RSC advances*, 2017, *7*, 45495-45503.

S9. Zhao, S., Chen, Y., & Song, Y. F. Tri-lacunary polyoxometalates of Na_8H $[PW_9O_{34}]$ as heterogeneous Lewis base catalysts for Knoevenagel condensation, cyanosilylation and the synthesis of benzoxazole derivatives. *Applied Catalysis A: General*, 2014, *475*, 140-146.

S10. Shahbazi, F., & Amani, K. Synthesis, characterization and heterogeneous catalytic activity of

diamine-modified silica-coated magnetite-polyoxometalate nanoparticles as a novel magnetically-recoverable nanocatalyst. *Catalysis Communications*, 2014, *55*, 57-64.

S11. Li, J., Wei, C., Han, Y., Mei, Y., Cheng, X., Huang, X., & Hu, C. Triazole-directed fabrication of polyoxovanadate-based metal–organic frameworks as efficient multifunctional heterogeneous catalysts for the Knoevenagel condensation and oxidation of alcohols. *Dalton Transactions*, 2021, *50*, 10082-10091.

S12. Lian, C., Li, H. L., & Yang, G. Y. High-Nuclear Ni-Substituted Poly (polyoxometalate) Containing an Anderson-like $\{Cs_7\}$ Cluster. *Inorganic Chemistry*, 2022, *61*, 11335-11341.

Table S6. Comparison of the catalytic activity of various POMs for the esterification Condensation reaction.

Catalyst	Catalyst dosage	Acid/MeOH (molar ratio)	Temperature (°C)	Time (h)	Yield (%)	Ref.
sulphated Zr-KIT-6	4 wt%	1:20	120	3	85	S13
SiW_{12}/Hβ	100 mg	1:20	60	10	90	S14
H_3PW/ ZrO_2	20 wt%	1:200	100	4	88	S15
WO_3/USY	10 wt %	1:6	200	2	74	S16
HPA/ZIF	3.3 wt%	1:60	Reflux	4	92	S17
Cu-SA	250 mg	1:10	50	1	50	S18
TPA_3/Hβ	-	1:60	60	6	84	S19
HPW@MIL-100	5 wt %	1:11	111	1	40	S20
$[Cu_2(BPPP)_2]\{\theta\text{-}[Mo_8O_{26}]\}$	0.20 mol %	1:12	63.0	4	97	This work

References:

S13. Gopinath, S., Kumar, P. S. M., Arafath, K. Y., Thiruvengadaravi, K. V., Sivanesan, S., & Baskaralingam, P. Efficient mesoporous SO_4^{2-}/Zr-KIT-6 solid acid catalyst for green diesel production from esterification of oleic acid. *Fuel*, 2017, *203*, 488-500.

S14. Narkhede, N., & Patel, A. Biodiesel production by esterification of oleic acid and transesterification of soybean oil using a new solid acid catalyst comprising 12-tungstosilicic acid and zeolite Hβ. *Industrial & Engineering Chemistry Research*, 2013, *52*, 13637-13644.

S15. Oliveira, C. F., Dezaneti, L. M., Garcia, F. A., de Macedo, J. L., Dias, J. A., Dias, S. C., & Alvim, K. S. Esterification of oleic acid with ethanol by 12-tungstophosphoric acid supported on zirconia. *Applied Catalysis A: General*, 2010, *372*, 153-161.

S16. Costa, A. A., Braga, P. R., de Macedo, J. L., Dias, J. A., & Dias, S. C. Structural effects of WO_3 incorporation on USY zeolite and application to free fatty acids esterification. *Microporous and mesoporous materials*, 2012, *147*, 142-148.

S17. Narenji-Sani, F., Tayebee, R., & Chahkandi, M. New task-specific and reusable ZIF-like grafted $H_6P_2W_{18}O_{62}$ catalyst for the effective esterification of free fatty acids. *ACS omega*, 2020, *5*, 9999-10010.

S18. Zhang, Q., Wei, F., Zhang, Y., Wei, F., Ma, P., Zheng, W., & Chen, H. Biodiesel production by catalytic esterification of oleic acid over copper(II)–alginate complexes. *Journal of Oleo Science*, 2017, *66*, 491-497.

S19. Patel, A., & Narkhede, N. 12-Tungstophosphoric acid anchored to zeolite Hβ: synthesis, characterization, and biodiesel production by esterification of oleic acid with methanol. *Energy & fuels*, 2012, *26*, 6025-6032.

S20. Wan, H., Chen, C., Wu, Z., Que, Y., Feng, Y., Wang, W., & Liu, X. Encapsulation of heteropolyanion-based ionic liquid within the metal–organic framework MIL-100 (Fe) for biodiesel production. *ChemCatChem*, 2015, *7*, 441-449.

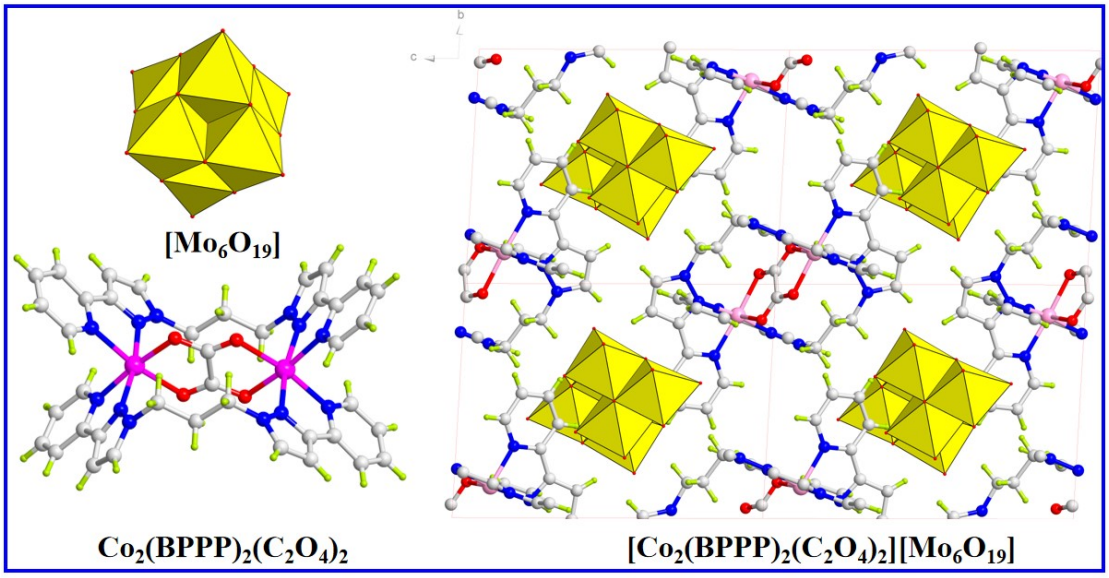

Figure S1. The $Co_2(BPPP)_2(C_2O_4)_2$ fragment, $[Mo_6O_{19}]$ cluster and the open network of $[Co_2(BPPP)_2(C_2O_4)_2][Mo_6O_{19}]$.

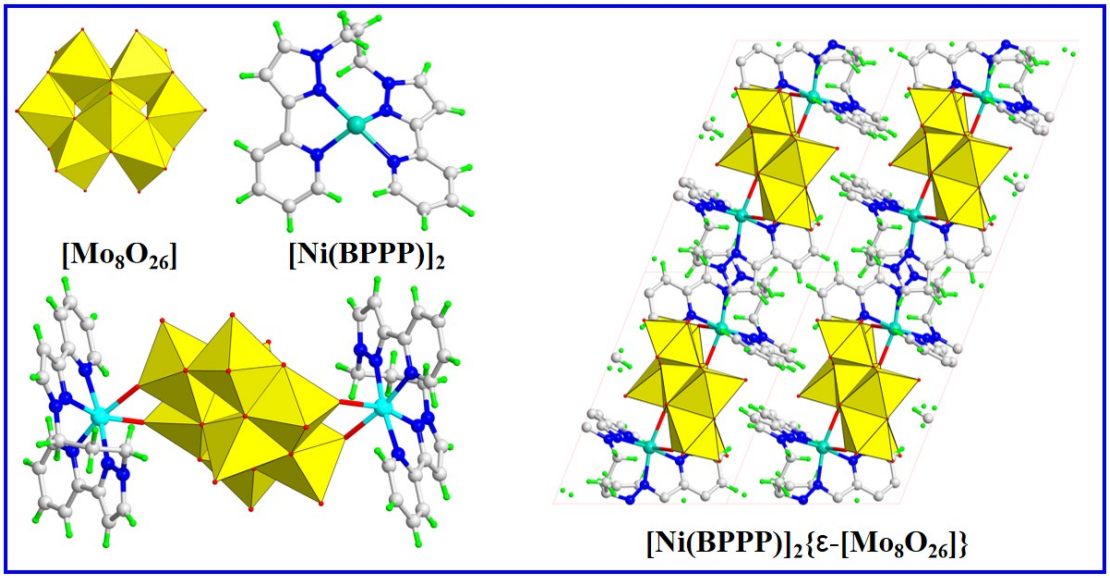

Figure S2. The $[Ni(BPPP)]_2$ fragment, $[Mo_8O_{26}]$ cluster and the open network of $[Ni(BPPP)]_2\{\varepsilon\text{-}[Mo_8O_{26}]\}$.

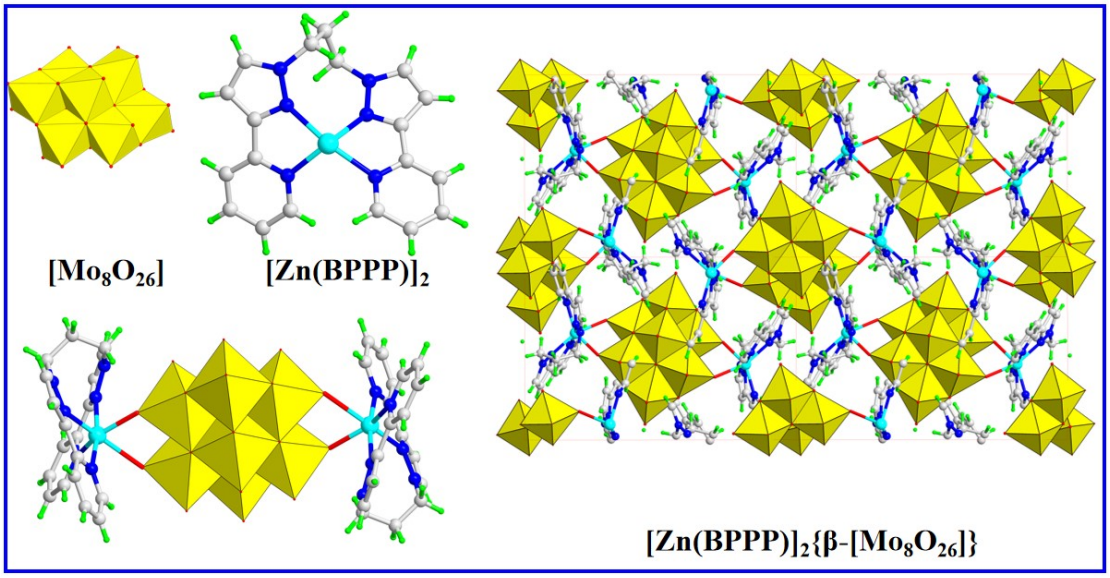

Figure S3. The $[Zn(BPPP)]_2$ fragment, $[Mo_8O_{26}]$ cluster and the 3D open network of $[Zn(BPPP)]_2\{\beta\text{-}[Mo_8O_{26}]\}$.

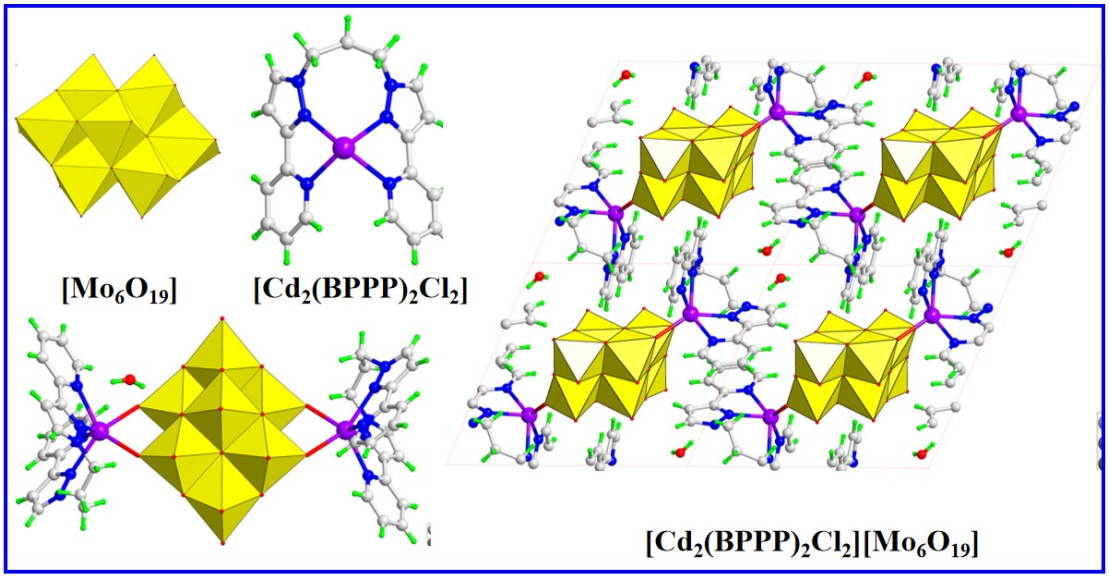

Figure S4. The $[Cd_2(BPPP)_2Cl_2]$ fragment, $[Mo_6O_{19}]$ cluster and the 3D open network of and $[Cd_2(BPPP)_2Cl_2][Mo_6O_{19}]$.

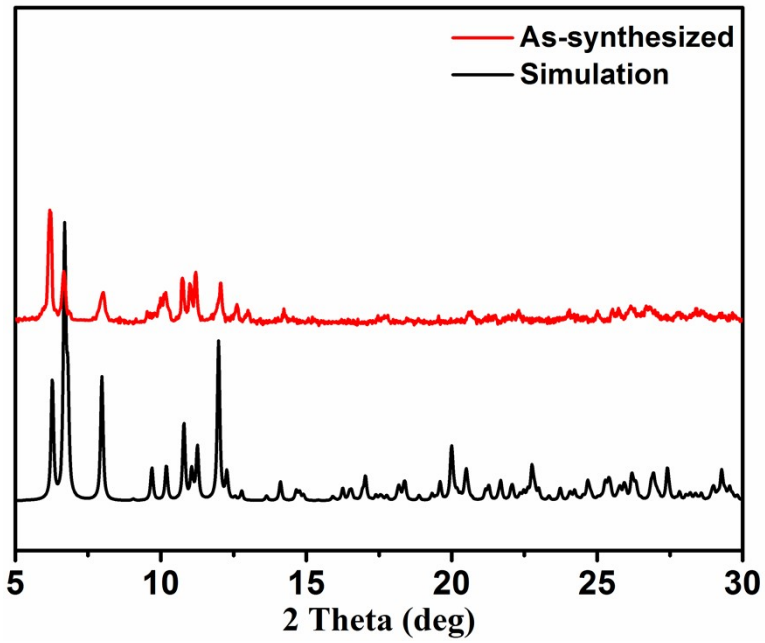

Figure S5. The PXRD patterns of as-synthesized **NUC-62** and simulated one.

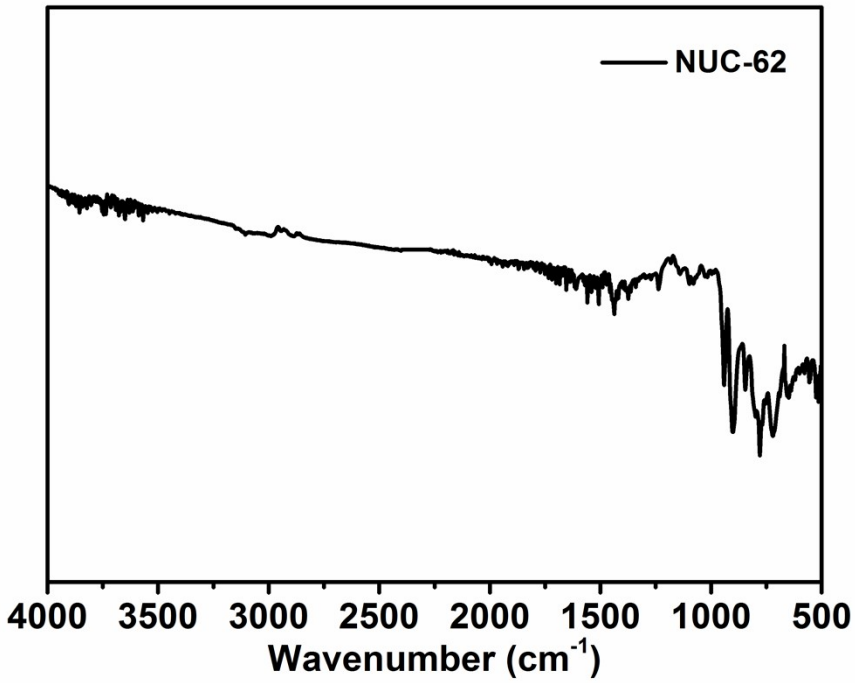

Figure S6. The FT-IR spectrum of as-synthesized **NUC-62**.

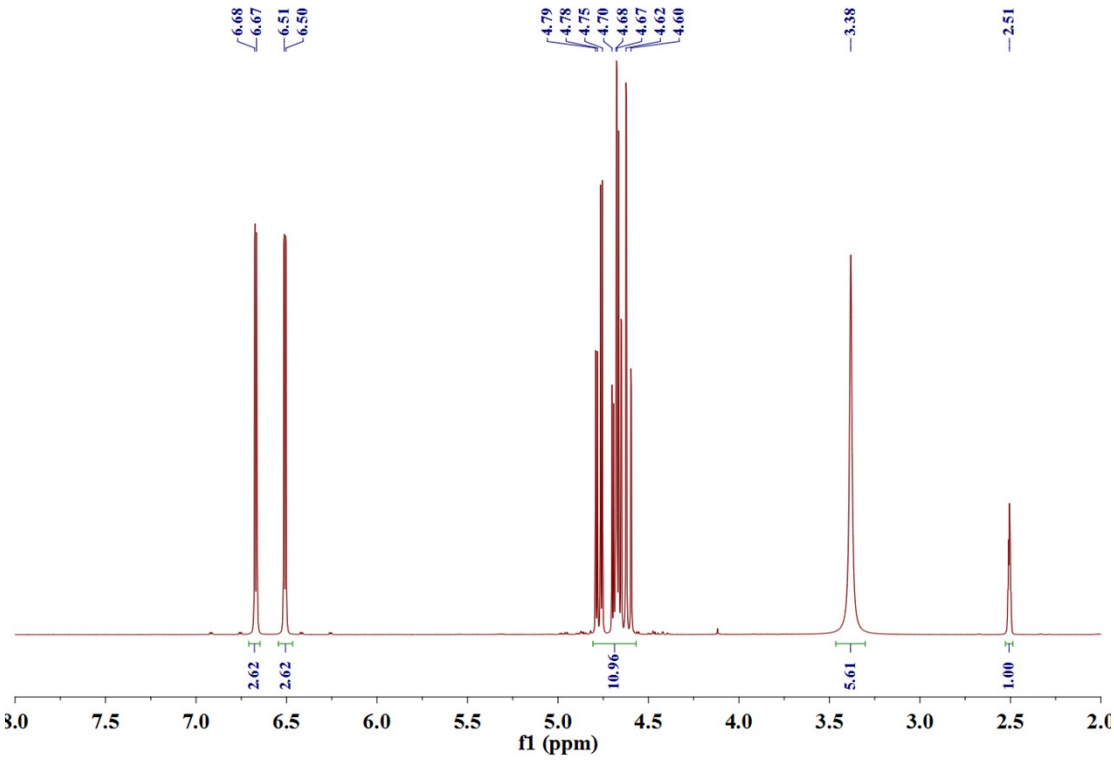

Figure S7. ^{1}H NMR spectrum of 4-fluoro-1,3-dioxolan-2-one.

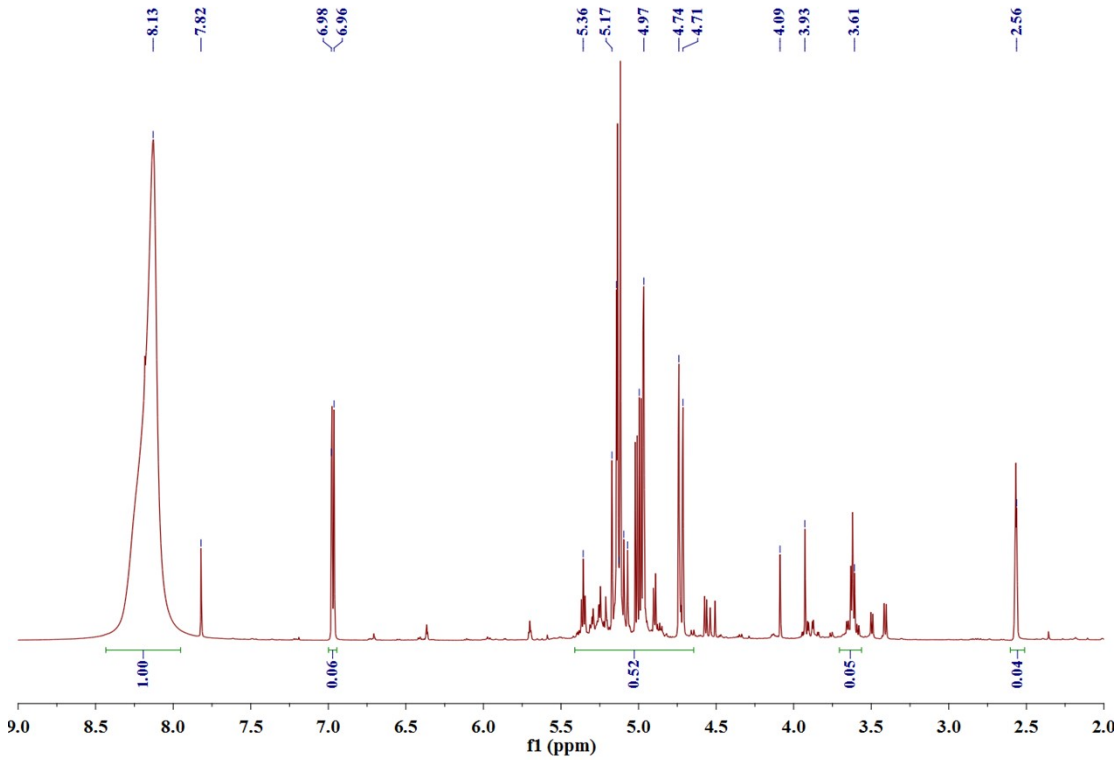

Figure S8. ^{1}H NMR spectrum of 4-chloro-1,3-dioxolan-2-one.

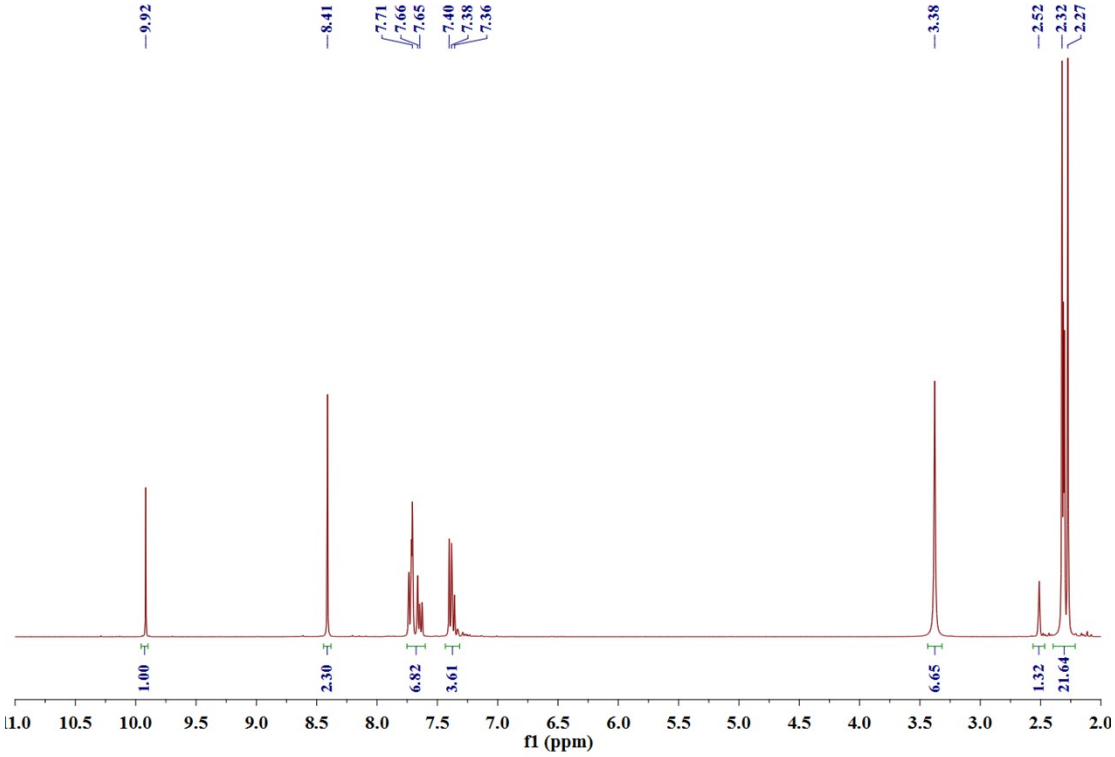

Figure S9. ^{1}H NMR spectrum of 4-methyl-1,3-dioxolan-2-one.

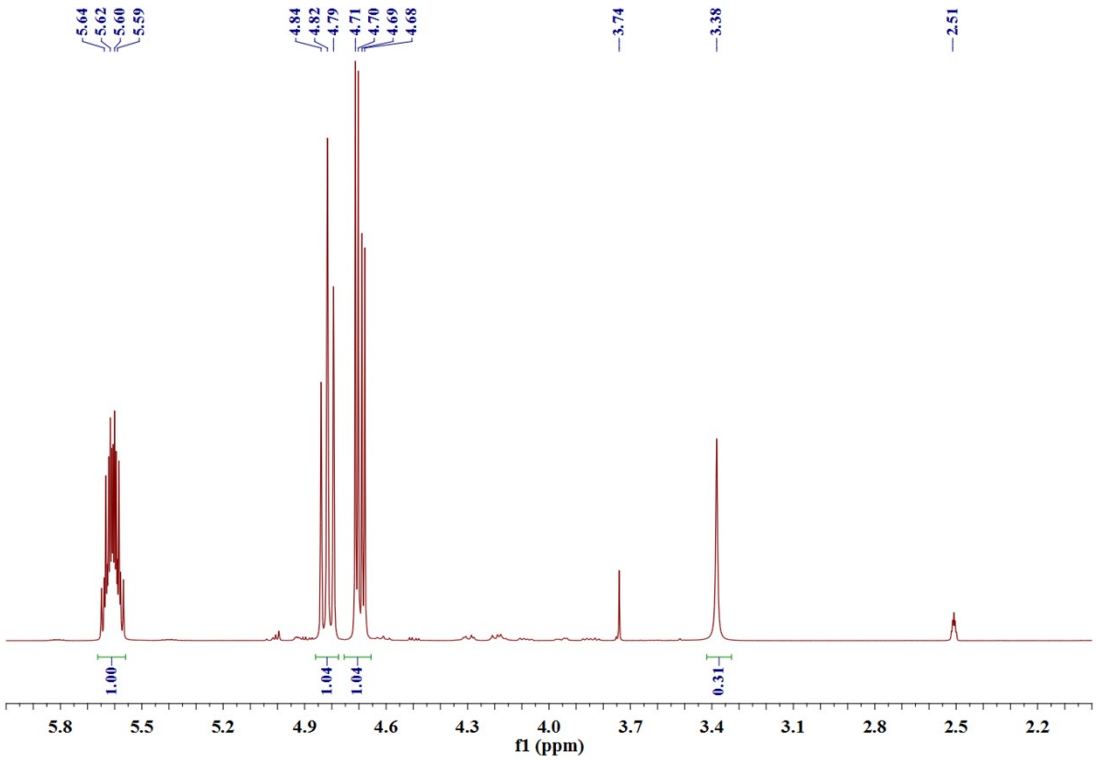

Figure S10. ^{1}H NMR spectrum of 4-(trifluoromethyl)-1,3-dioxolan-2-one.

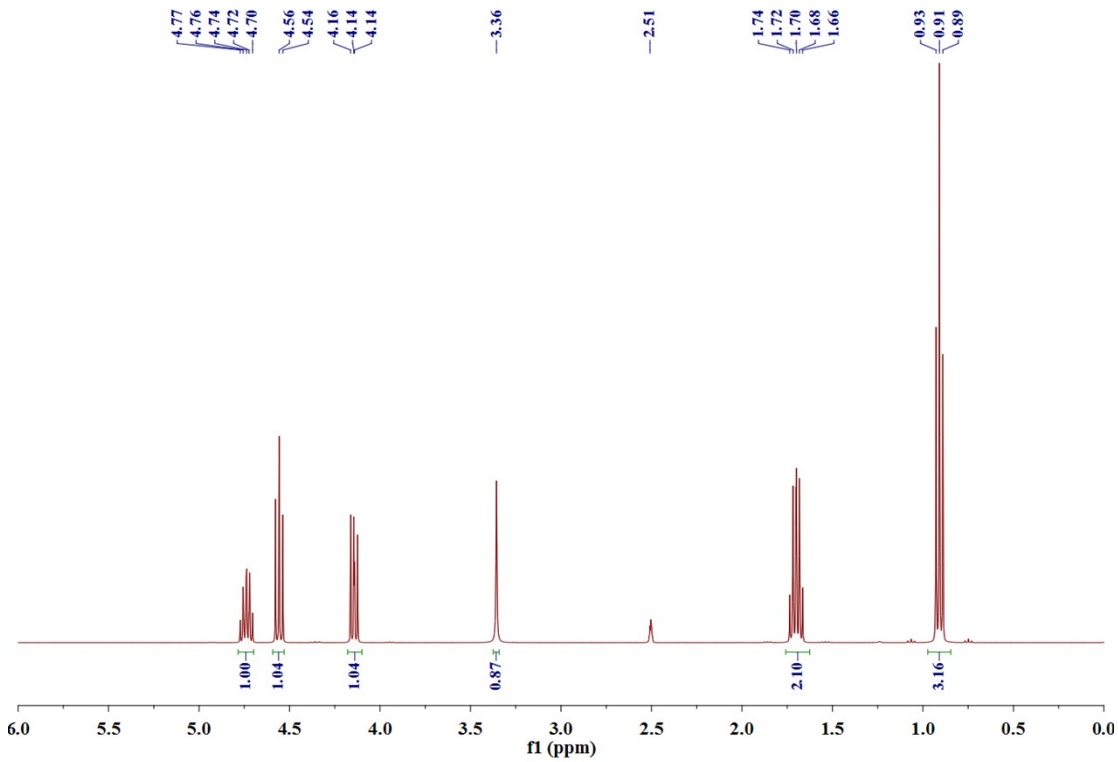

Figure S11. ^{1}H NMR spectrum of 4-ethyl-1,3-dioxolan-2-one.

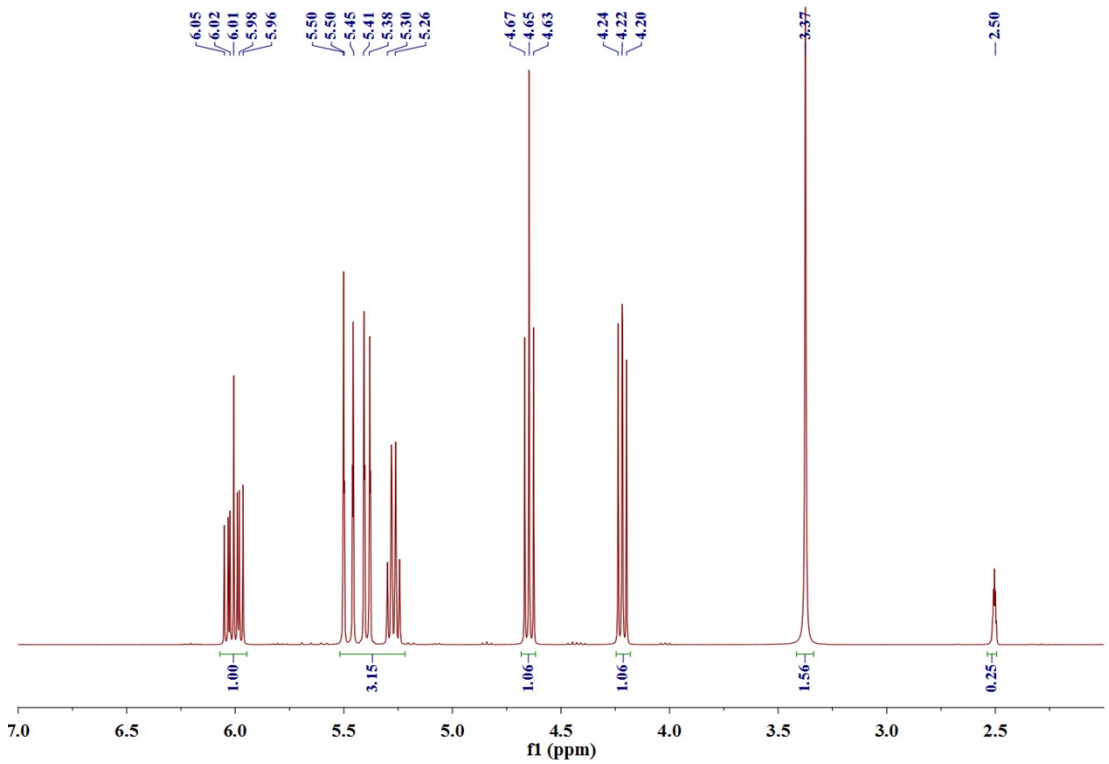

Figure S12. ^{1}H NMR spectrum of 4-ethenyl-1,3-dioxolan-2-one.

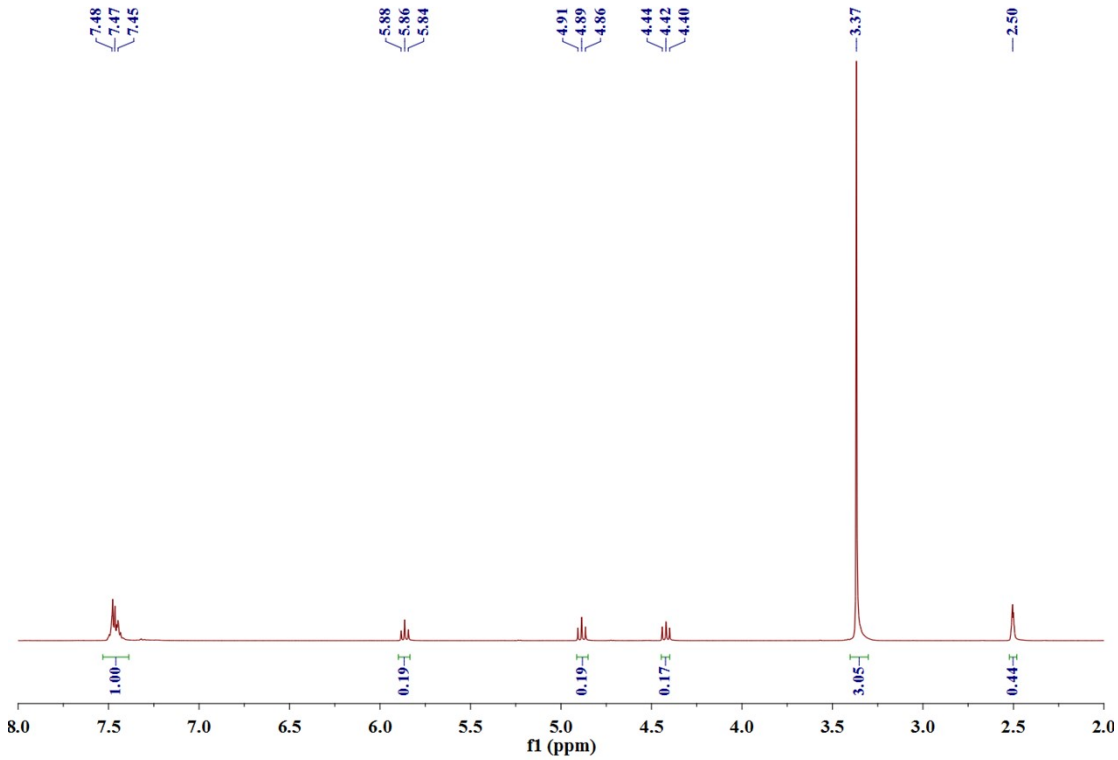

Figure S13. ^{1}H NMR spectrum of 4-benzyl-1,3-dioxolan-2-one.

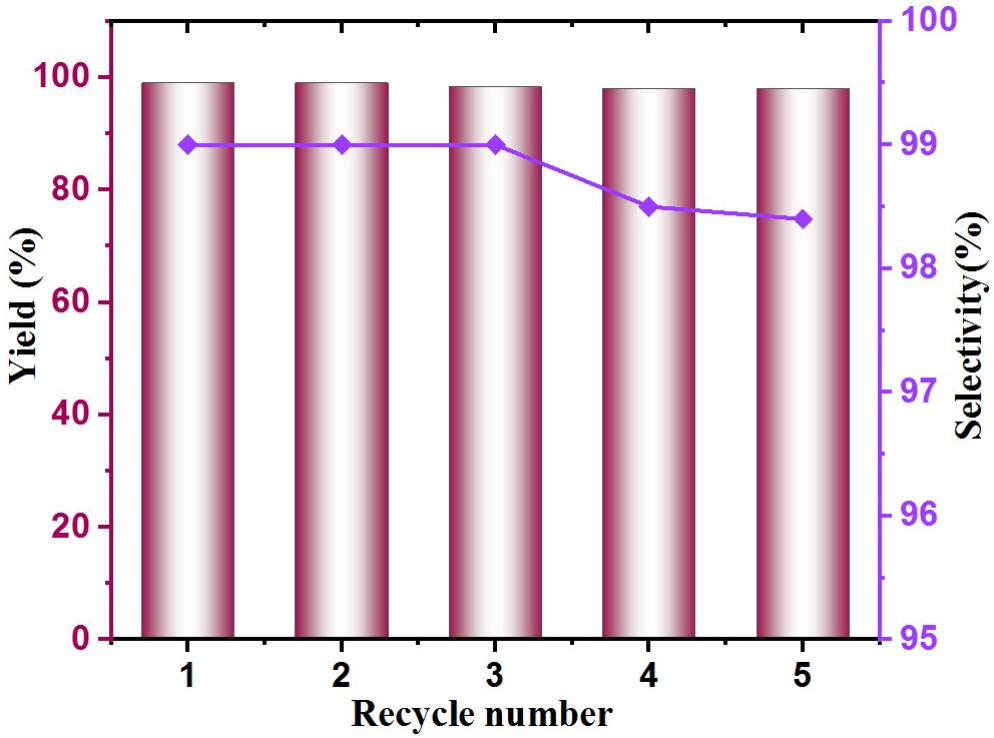

Figure S14. Recyclability study (five cycles) for catalytic activities of **NUC-62** in cycloaddition reaction.

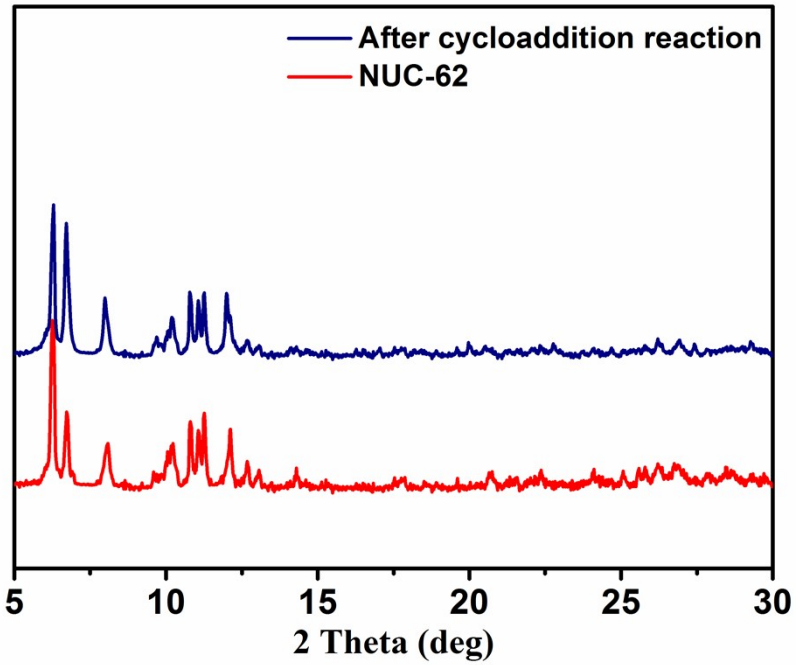

Figure S15. The PXRD patterns of **NUC-62** and used **NUC-62** after fifth cycloaddition reactions.

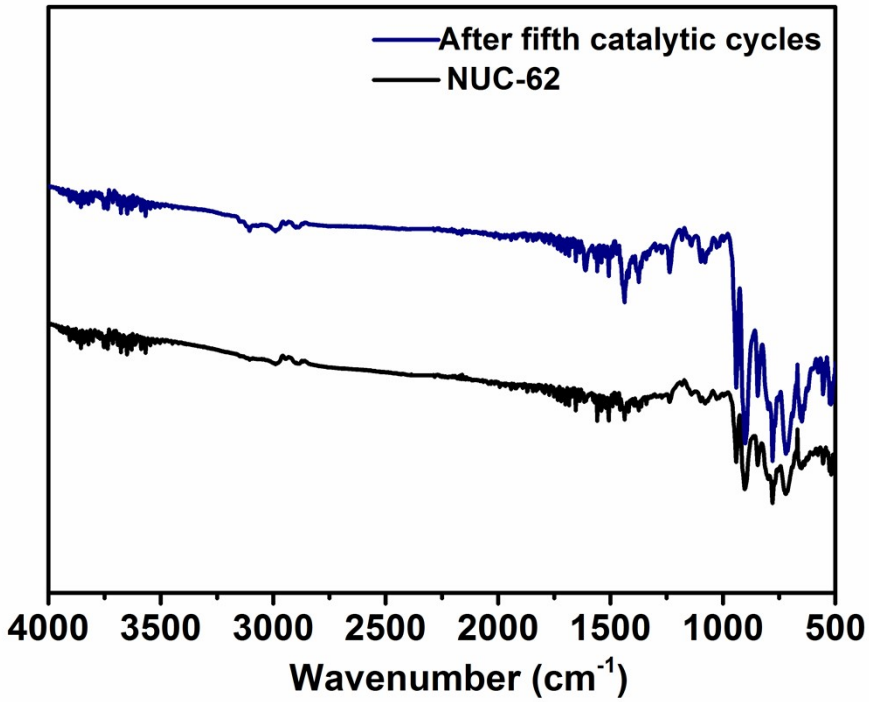

Figure S16. The FT-IR patterns of **NUC-62** and used **NUC-62** after fifth cycloaddition reactions.

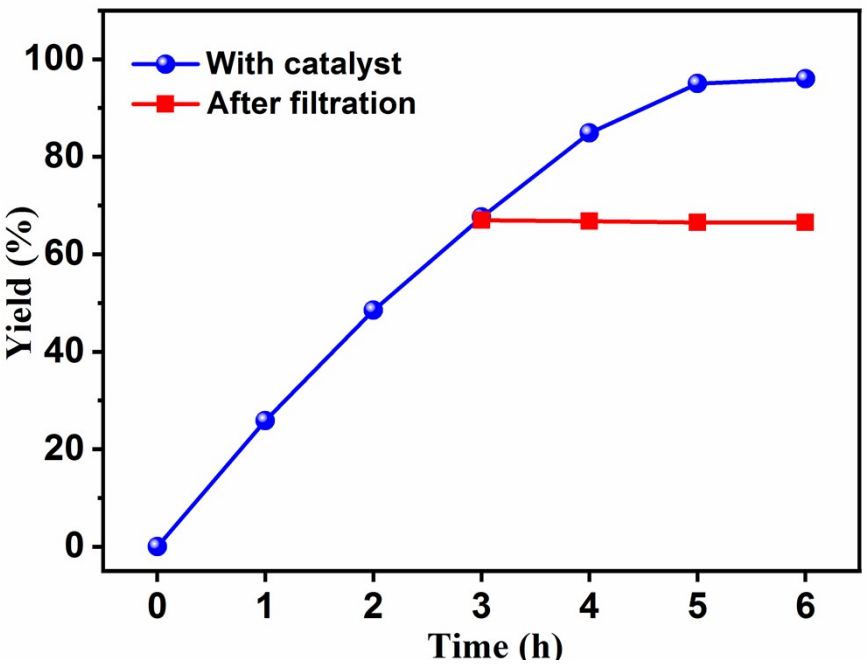

Figure S17. Evidence of heterogeneous nature of **NUC-62** in the cycloaddition reaction.

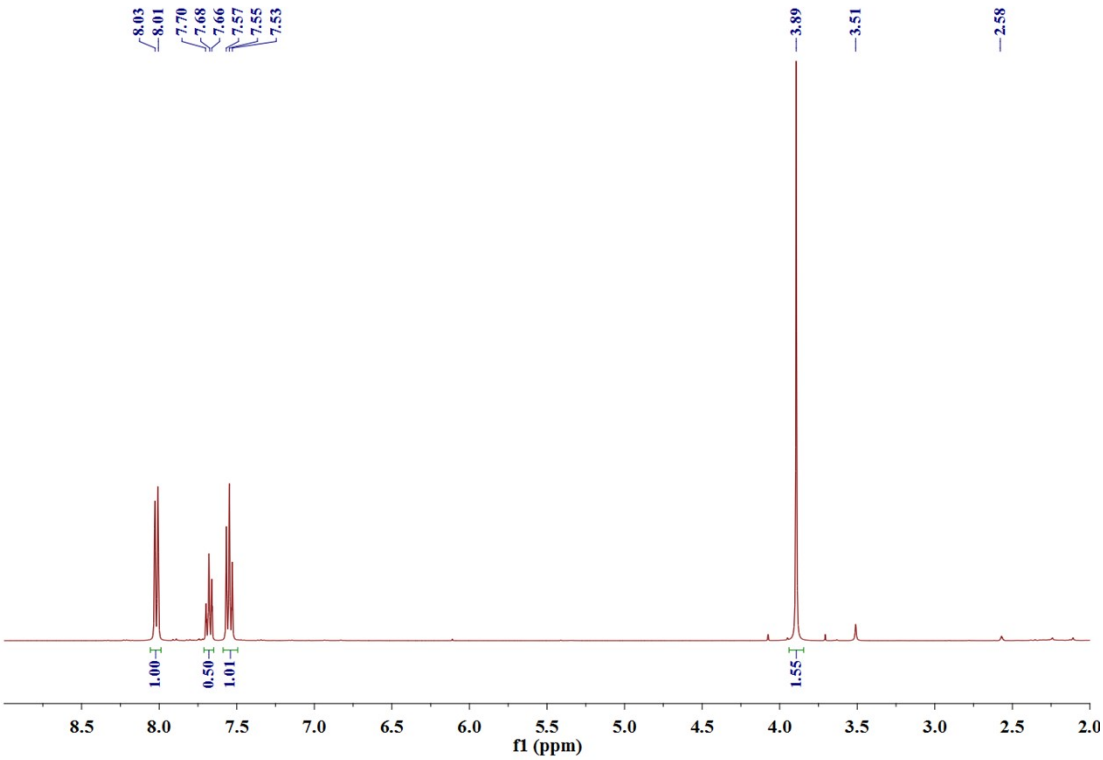

Figure S18. ^{1}H NMR spectrum of methyl benzoate.

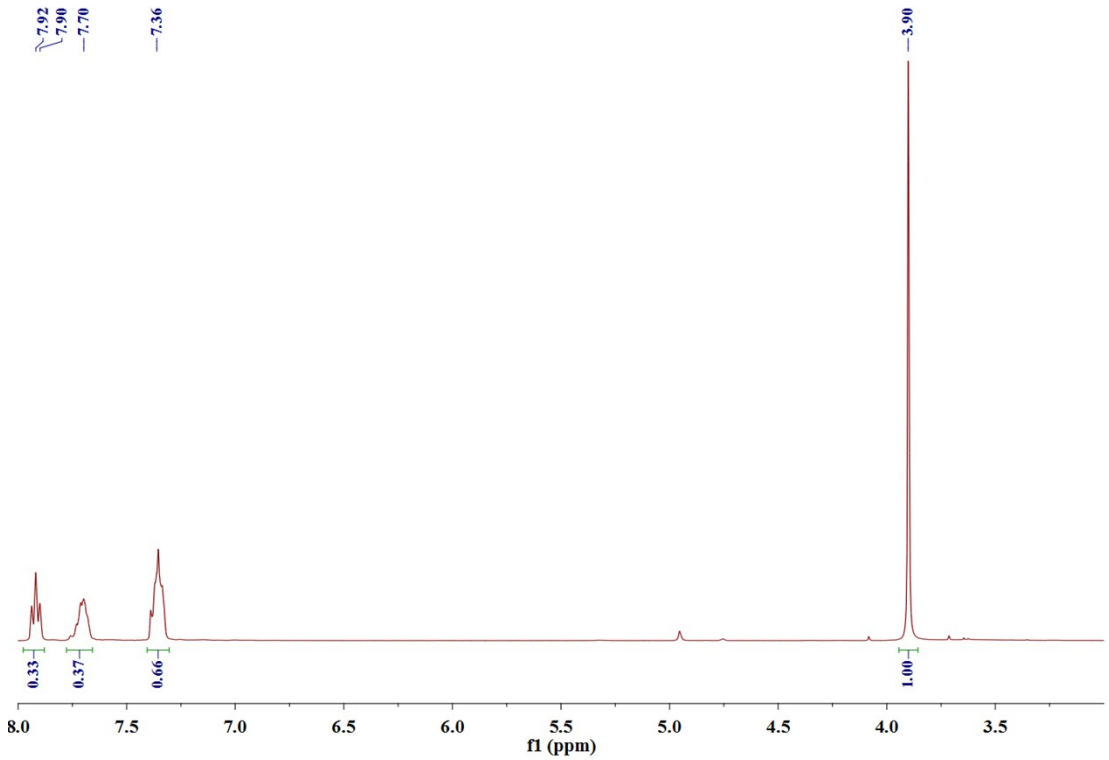

Figure S19. ^{1}H NMR spectrum of methyl 4-fluorobenzoate.

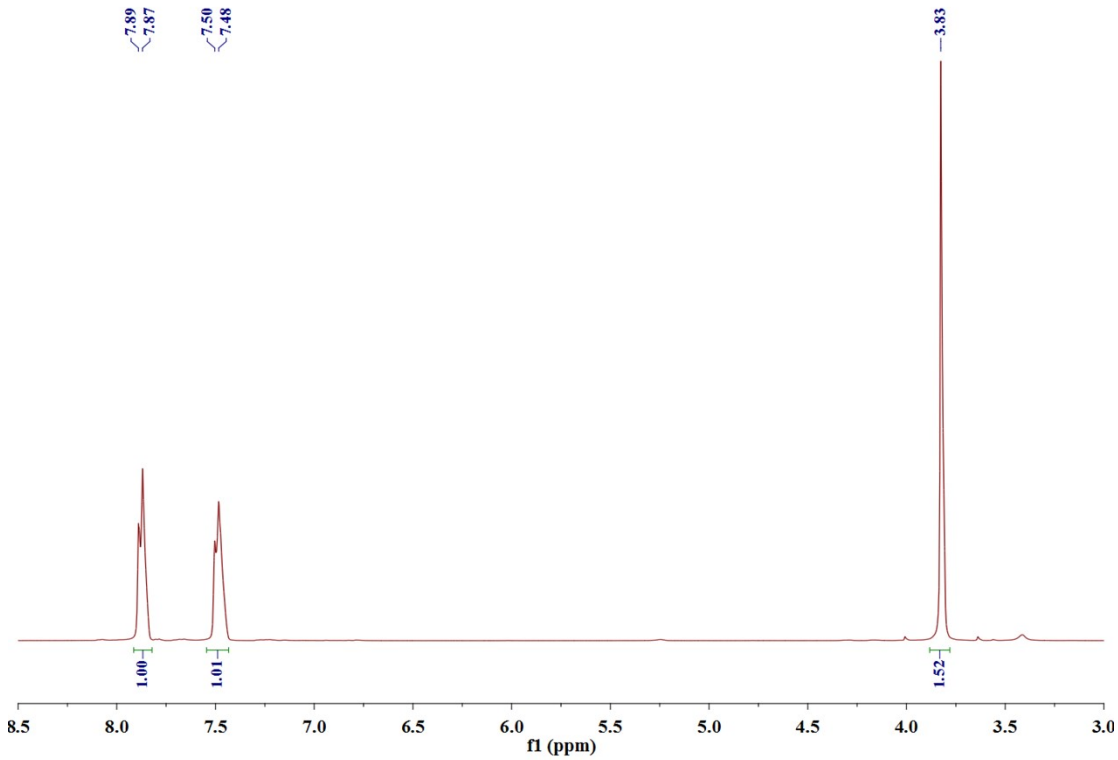

Figure S20. ^{1}H NMR spectrum of methyl 4-chlorobenzoate.

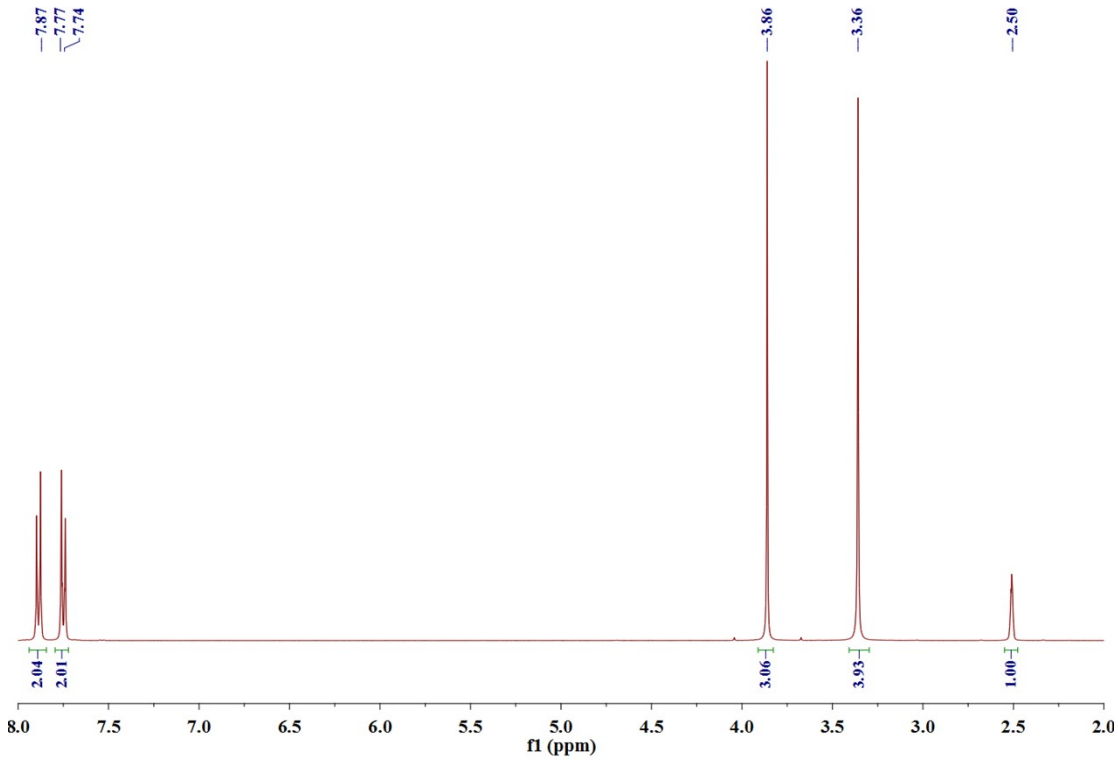

Figure S21. ^{1}H NMR spectrum of methyl 4-bromobenzoate.

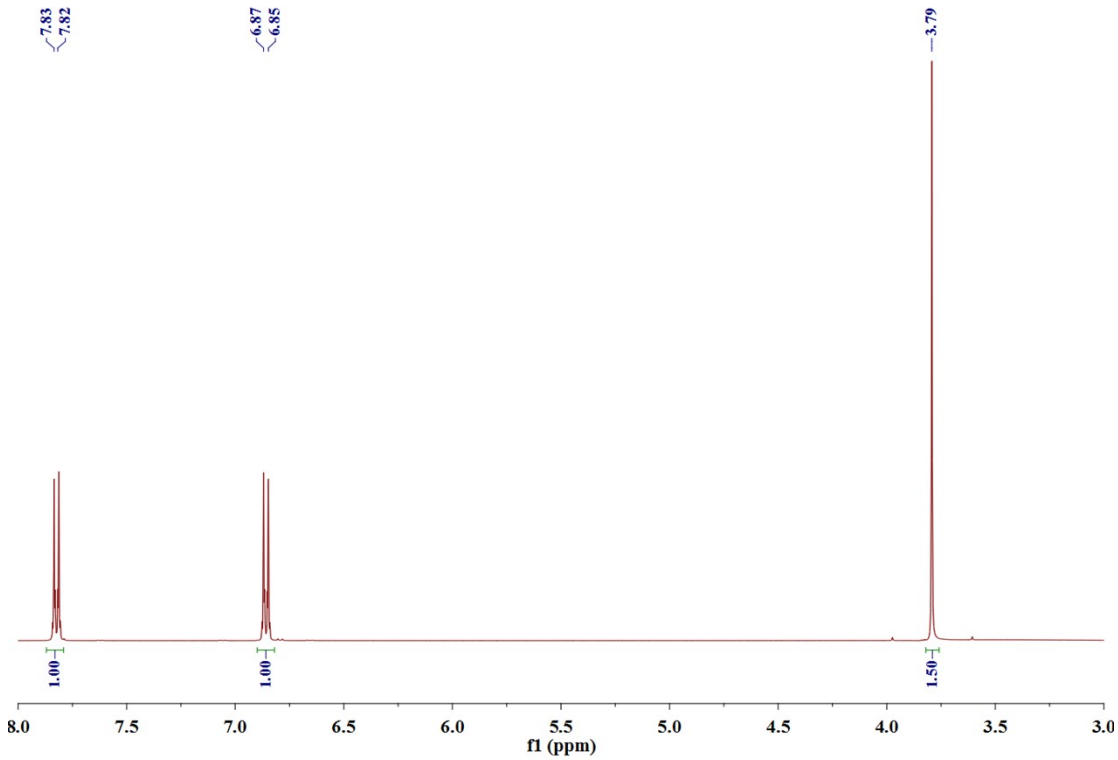

Figure S22. ^{1}H NMR spectrum of methyl 4-nitrobenzoate.

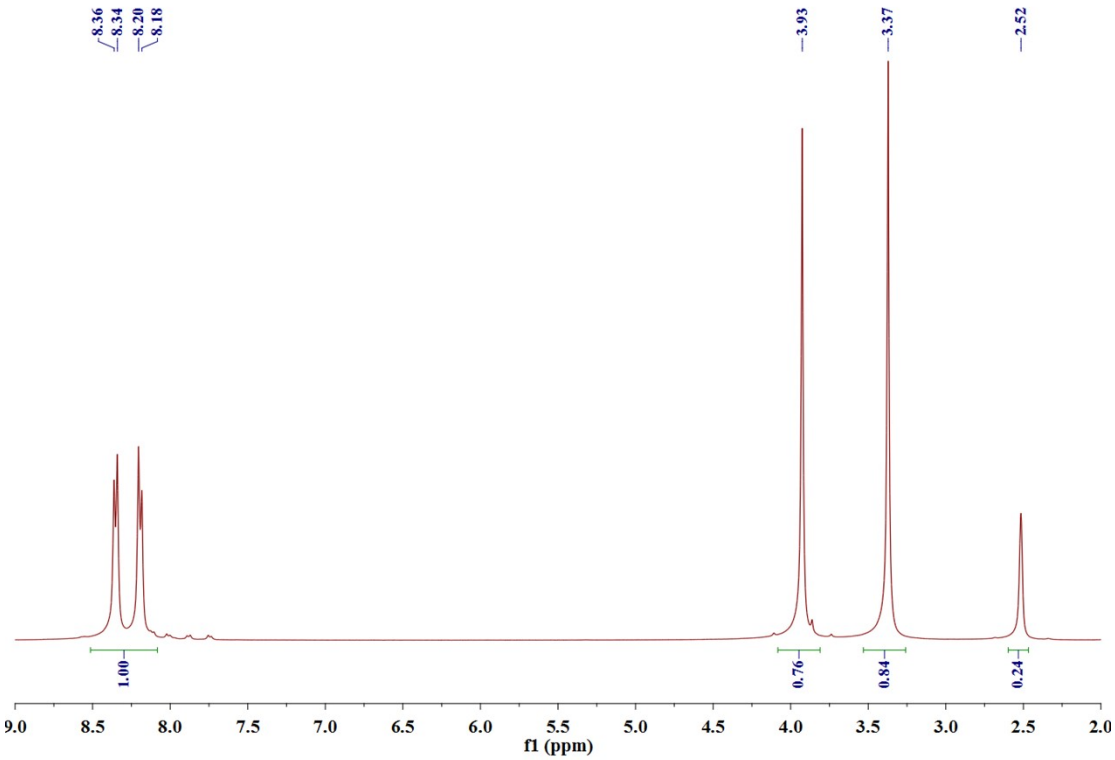

Figure S23. ^{1}H NMR spectrum of methyl 4-hydroxybenzoate.

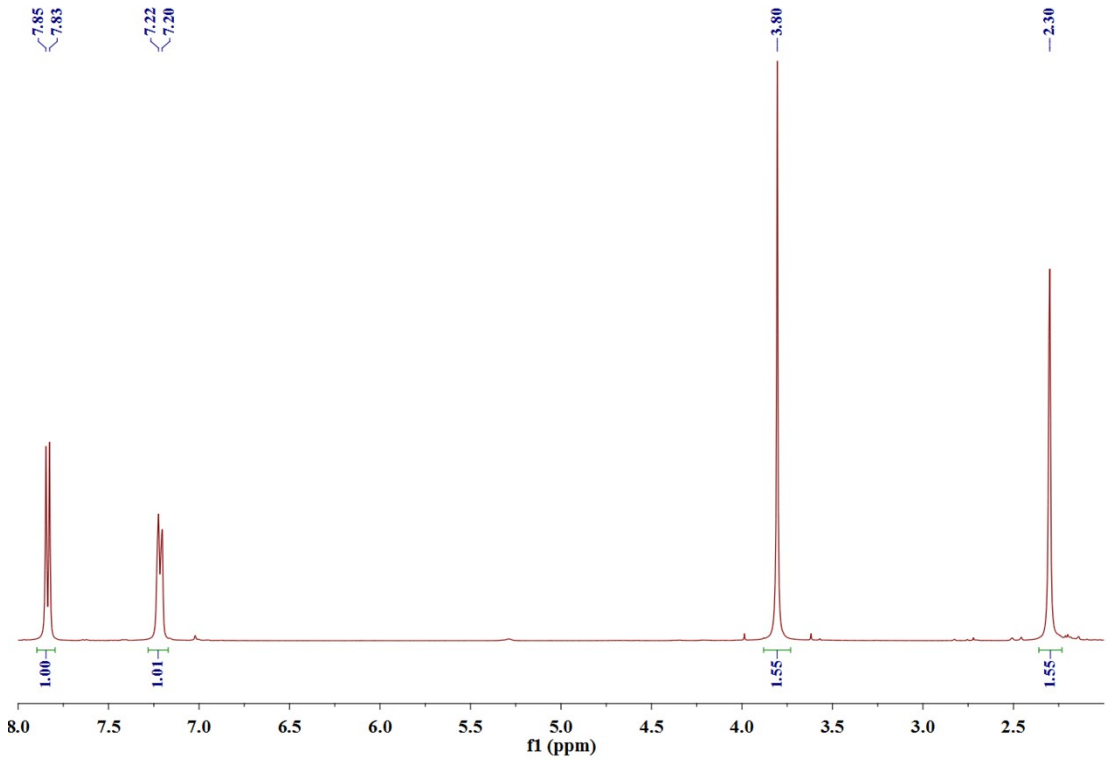

Figure S24. ^{1}H NMR spectrum of methyl 4-methylbenzoate.

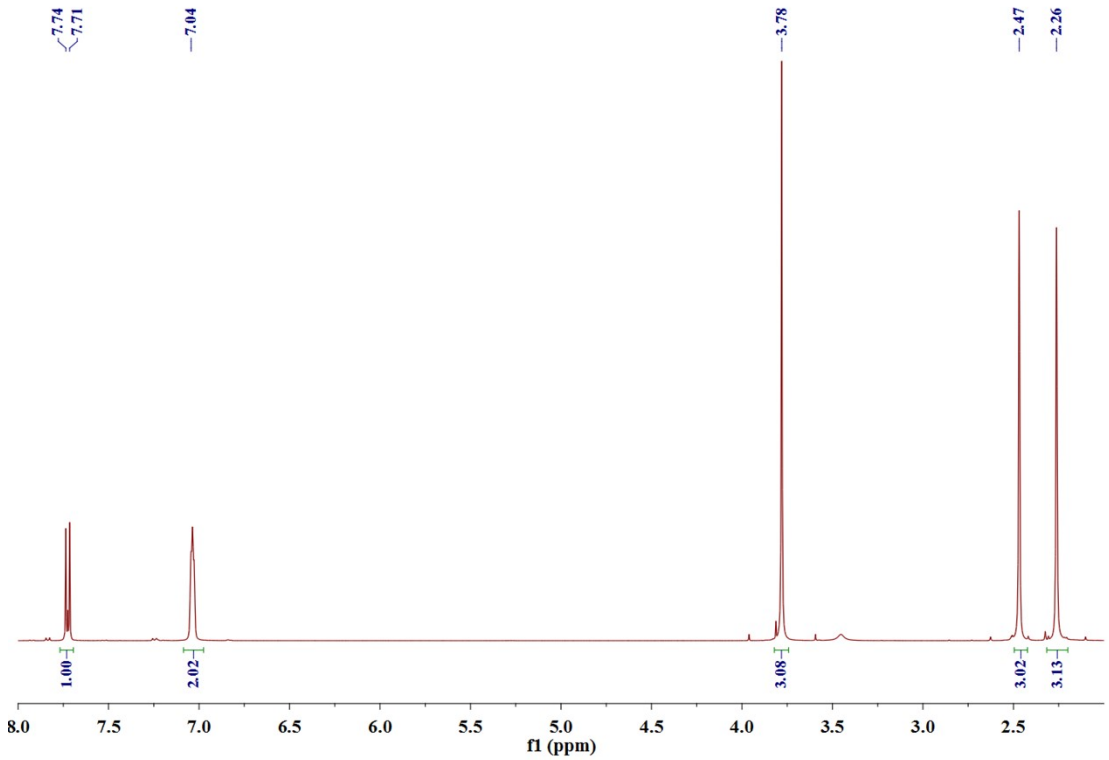

Figure S25. ^{1}H NMR spectrum of methyl 2,4-dimethylbenzoate.

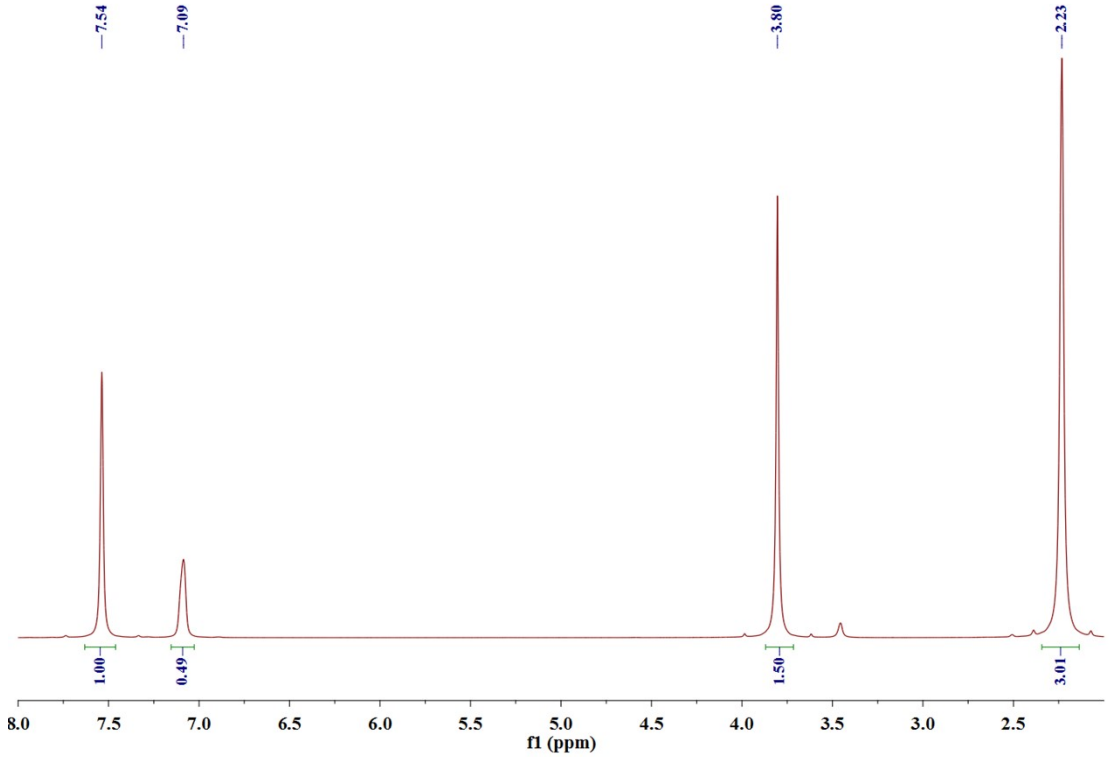

Figure S26. ^{1}H NMR spectrum of methyl 3,5-dimethylbenzoate.

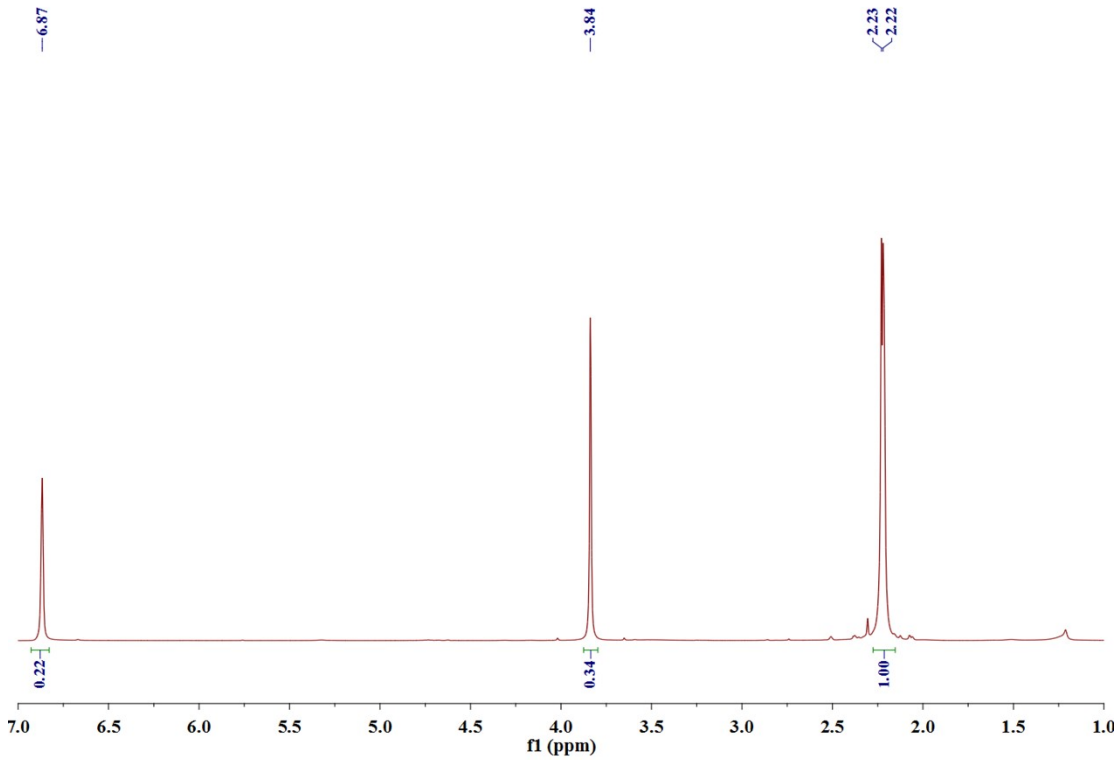

Figure S27. ^{1}H NMR spectrum methyl 2,4,6-trimethylbenzoate.

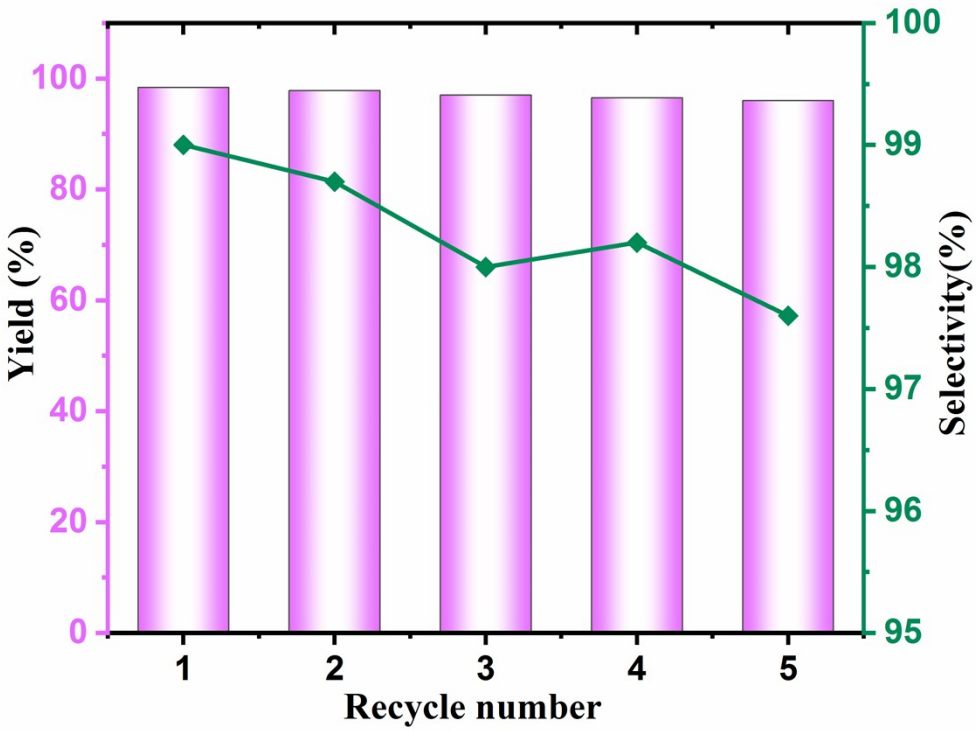

Figure S28. Recyclability study (five cycles) for catalytic activities of **NUC-62** in esterification condensation reaction.

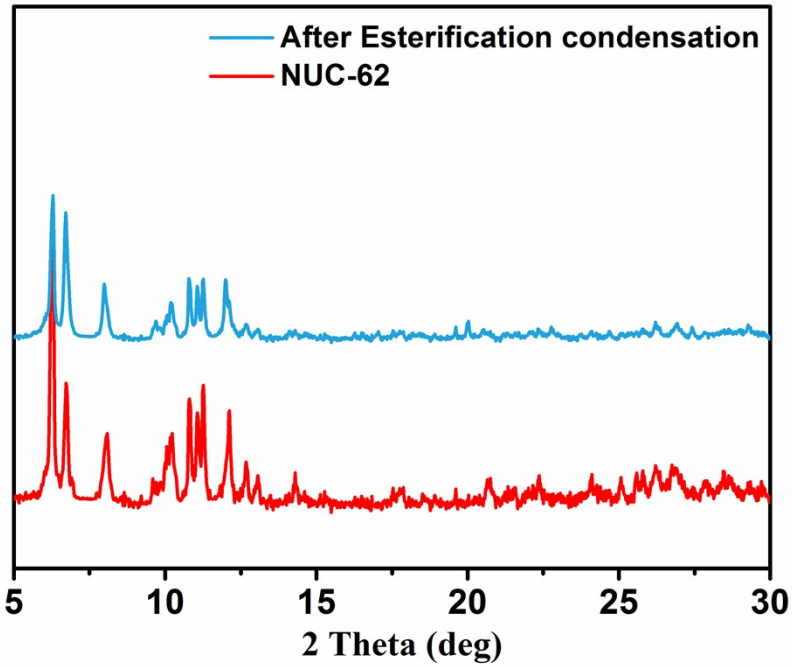

Figure S29. The PXRD patterns of **NUC-62** and used **NUC-62** after fifth esterification condensation reaction.

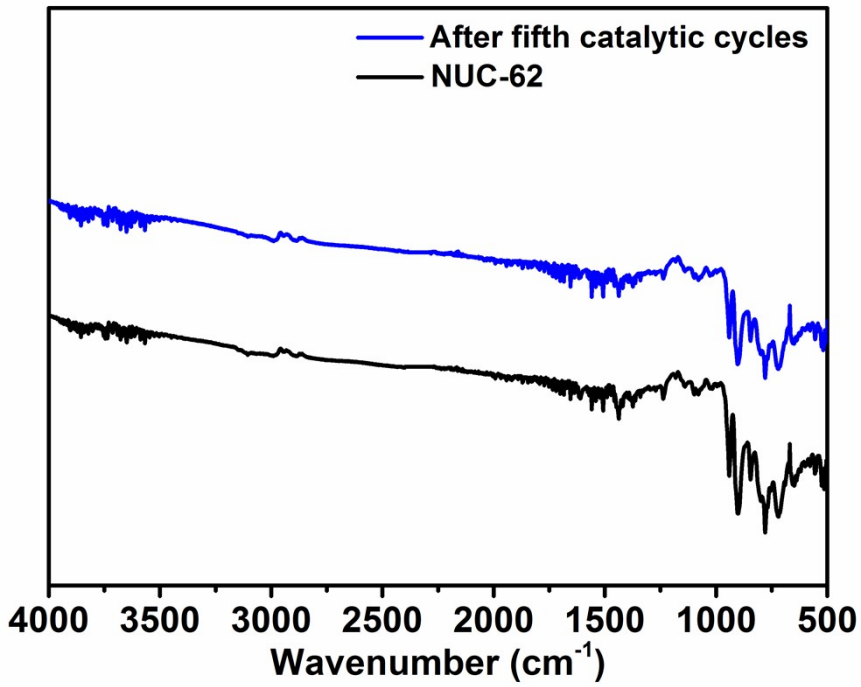

Figure S30. The FT-IR patterns of **NUC-62** and used **NUC-62** after fifth esterification condensation reaction.

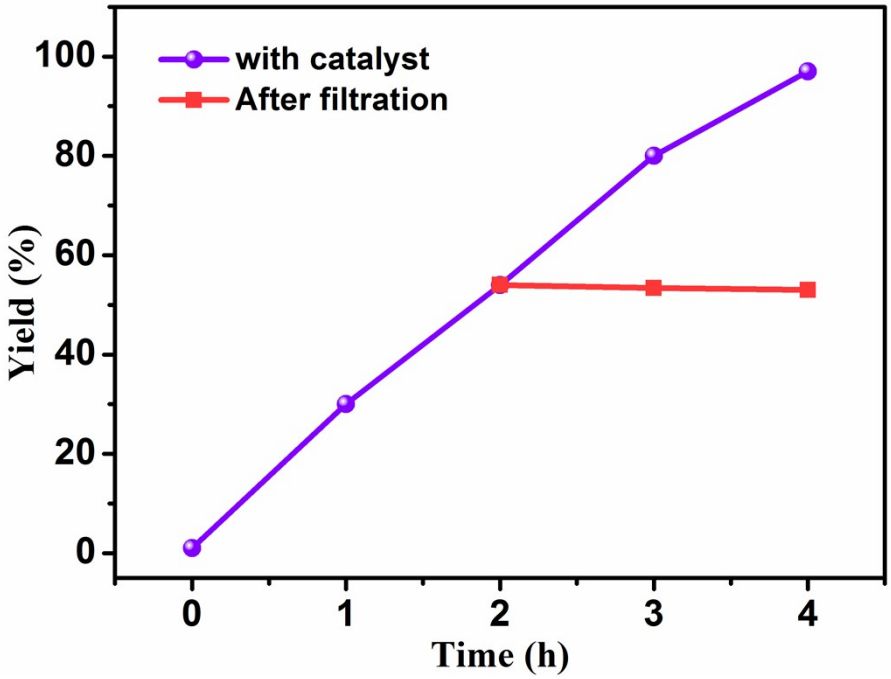

Figure S31. Evidence of heterogeneous nature of **NUC-62** in the esterification condensation reaction.

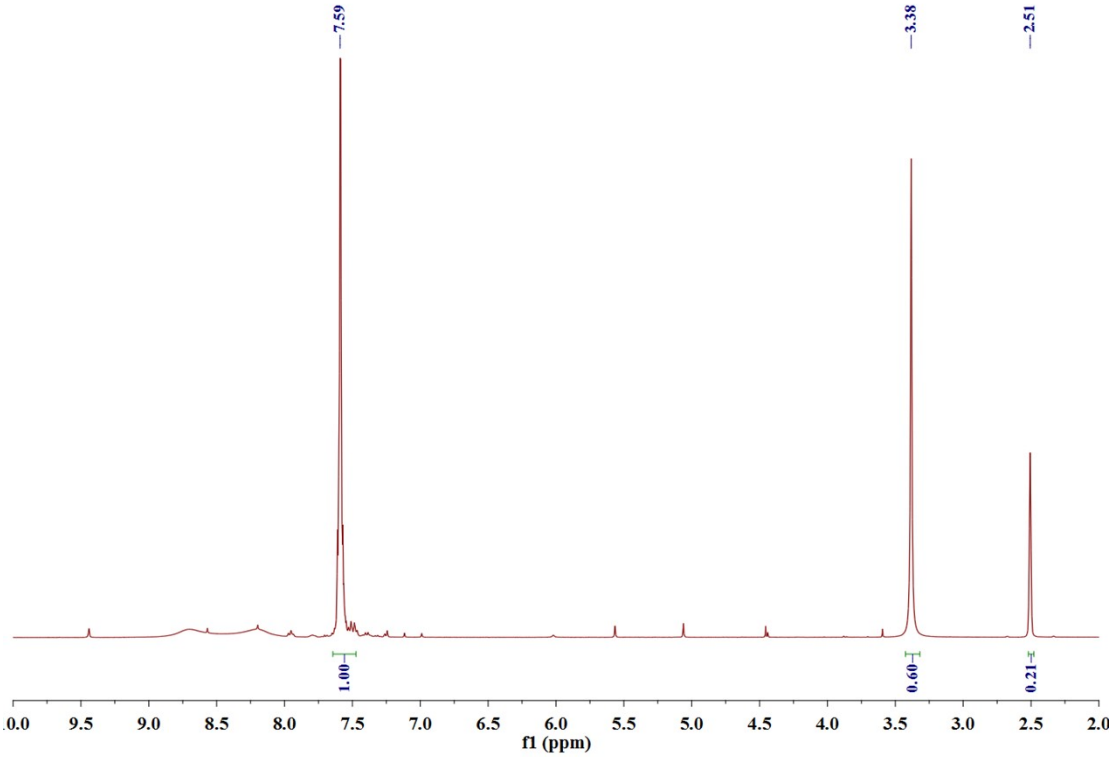

Figure S32. ^{1}H NMR spectrum of 2-(phenylmethylidene)propanedinitrile.

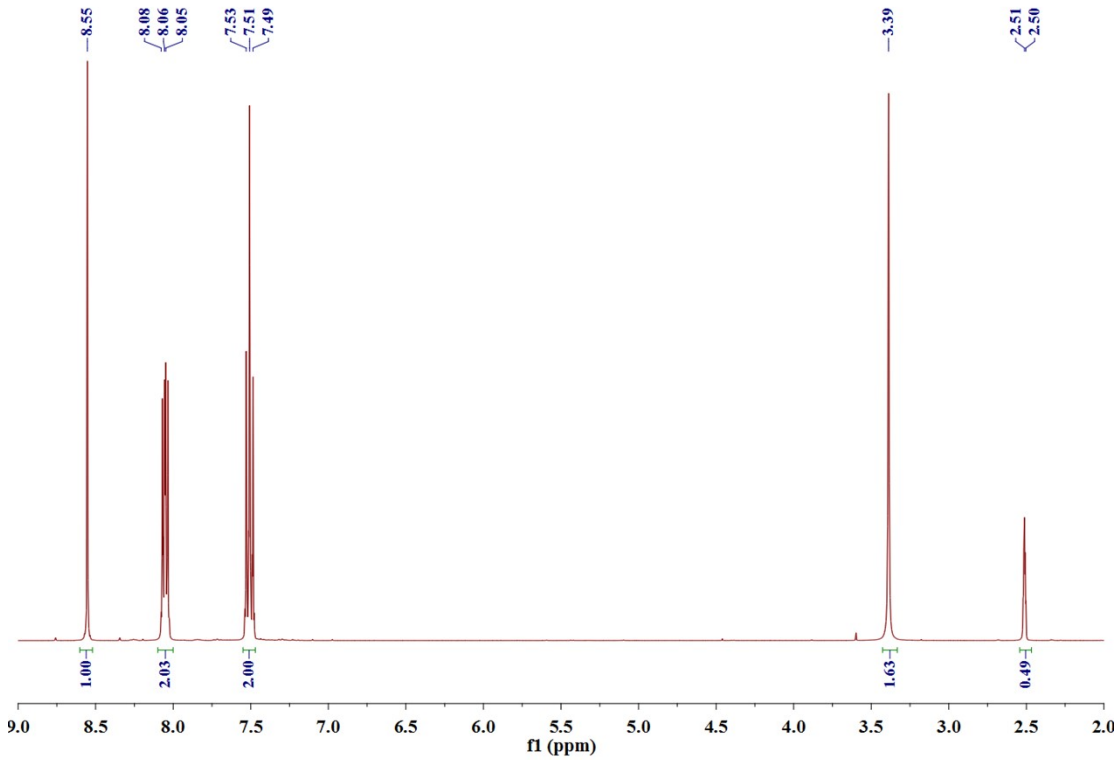

Figure S33. ^{1}H NMR spectrum of 2-[(4-fluorophenyl)methylidene]propanedinitrile.

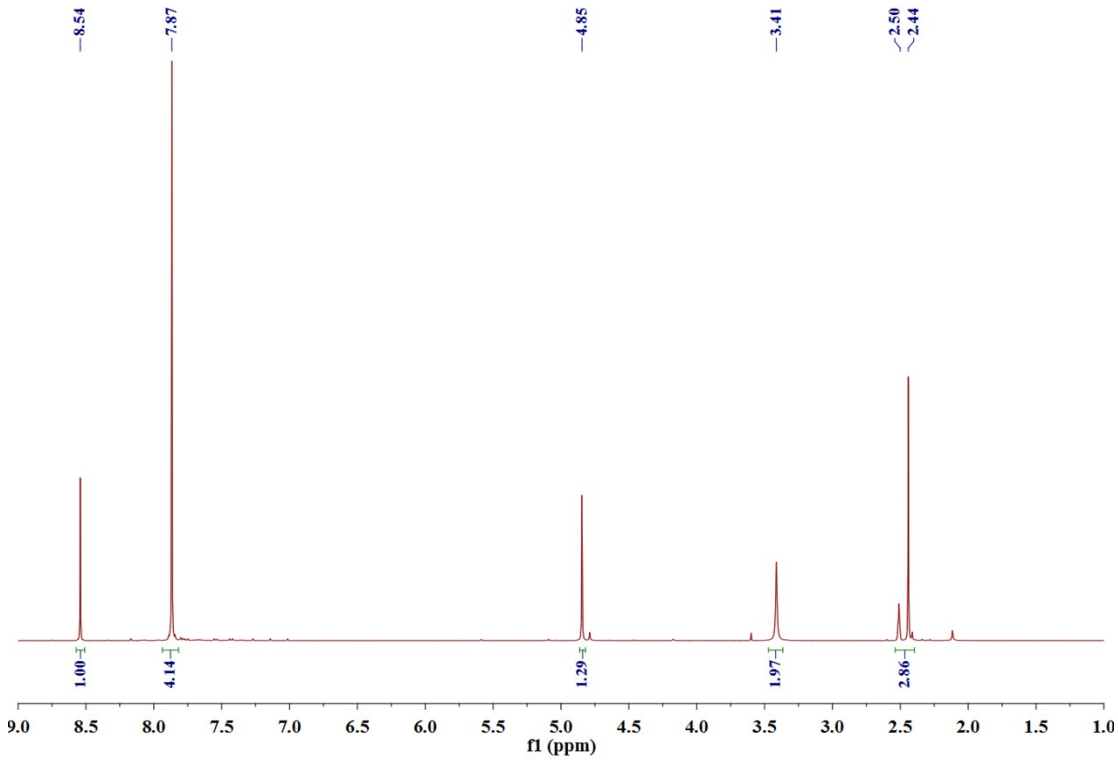

Figure S34. ^{1}H NMR spectrum of 2-[(4-chlorophenyl)methylidene]propanedinitrile.

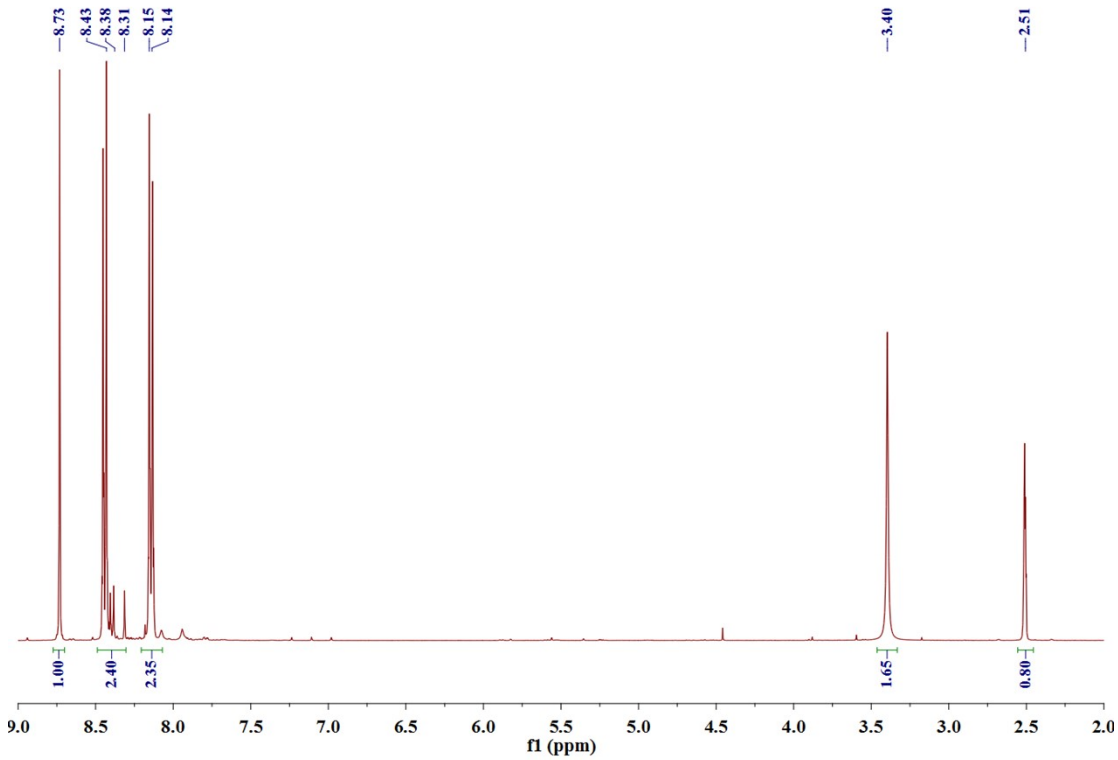

Figure S35. ^{1}H NMR spectrum of 2-[(4-nitrophenyl)methylidene]propanedinitrile.

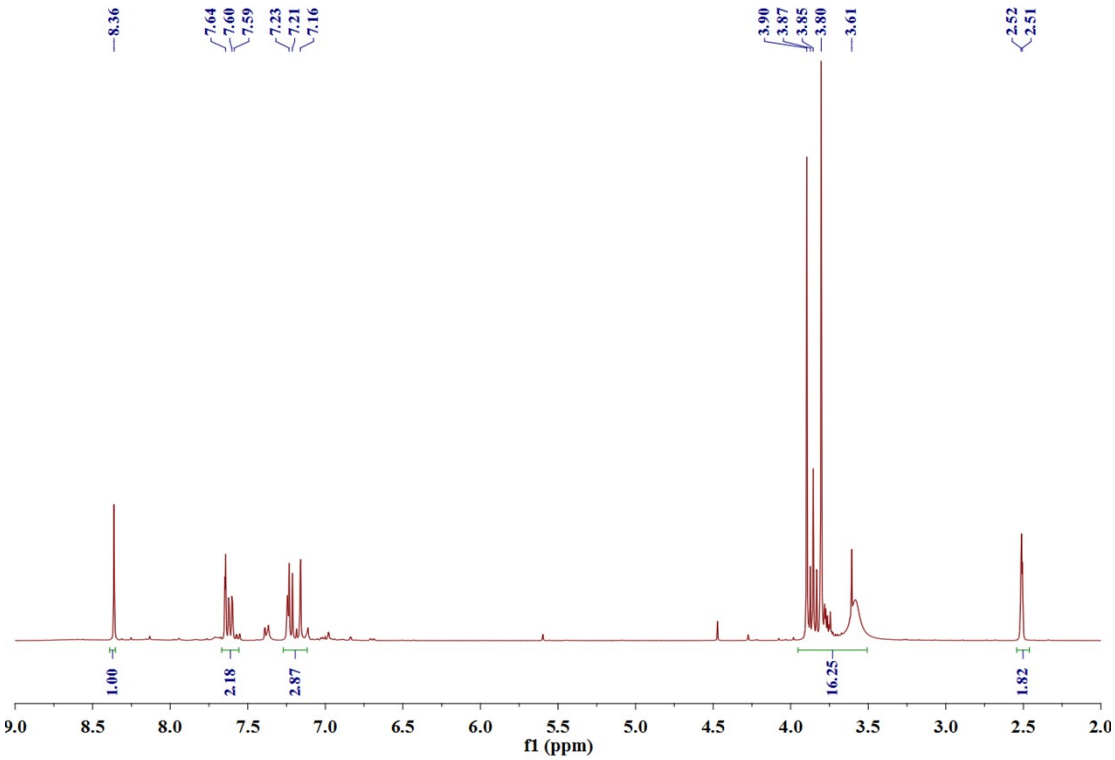

Figure S36. ^{1}H NMR spectrum of 2-[(3,4-dimethoxyphenyl)methylidene]propanedinitrile.

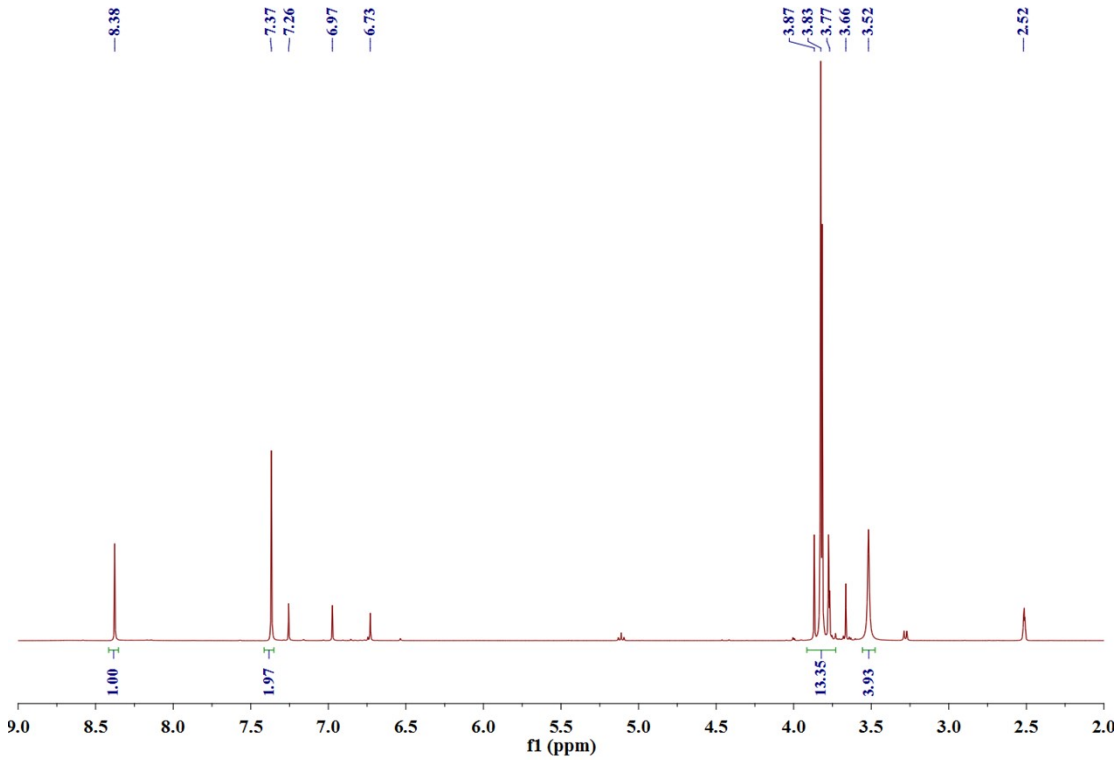

Figure S37. ^{1}H NMR spectrum of 2-[(3,4,5-trimethoxyphenyl)methylidene]propanedinitrile.

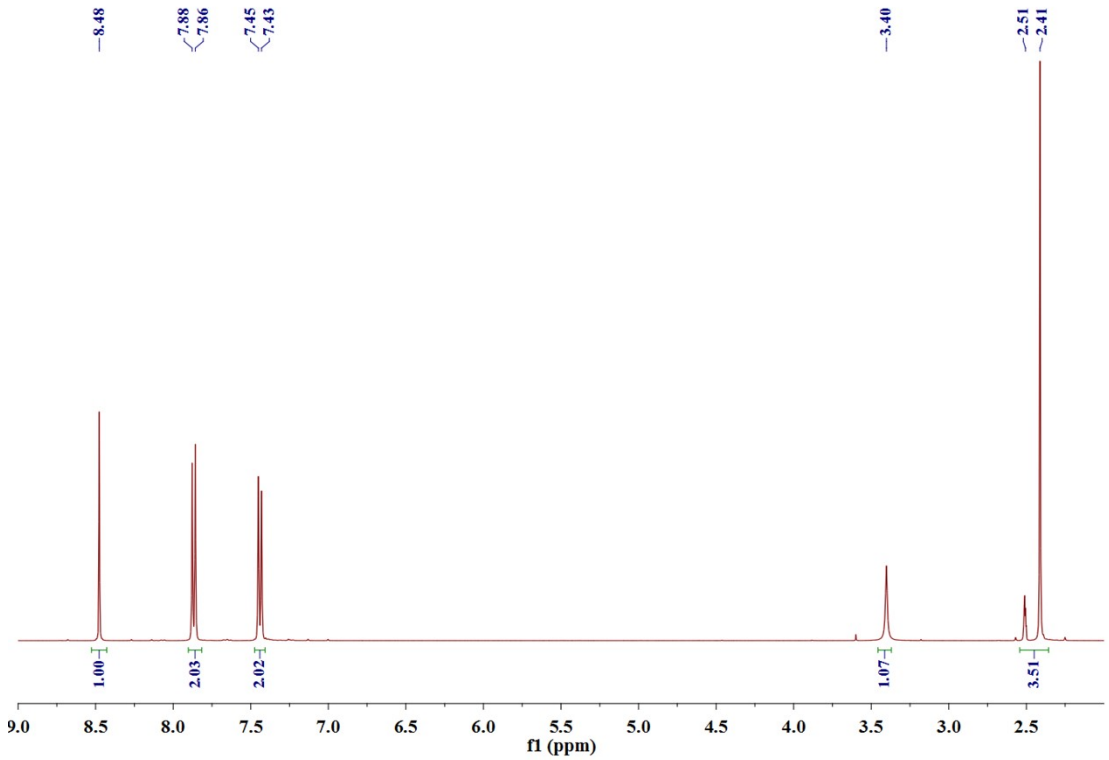

Figure S38. ^{1}H NMR spectrum of 2-[(4-methylphenyl)methylidene]propanedinitrile.

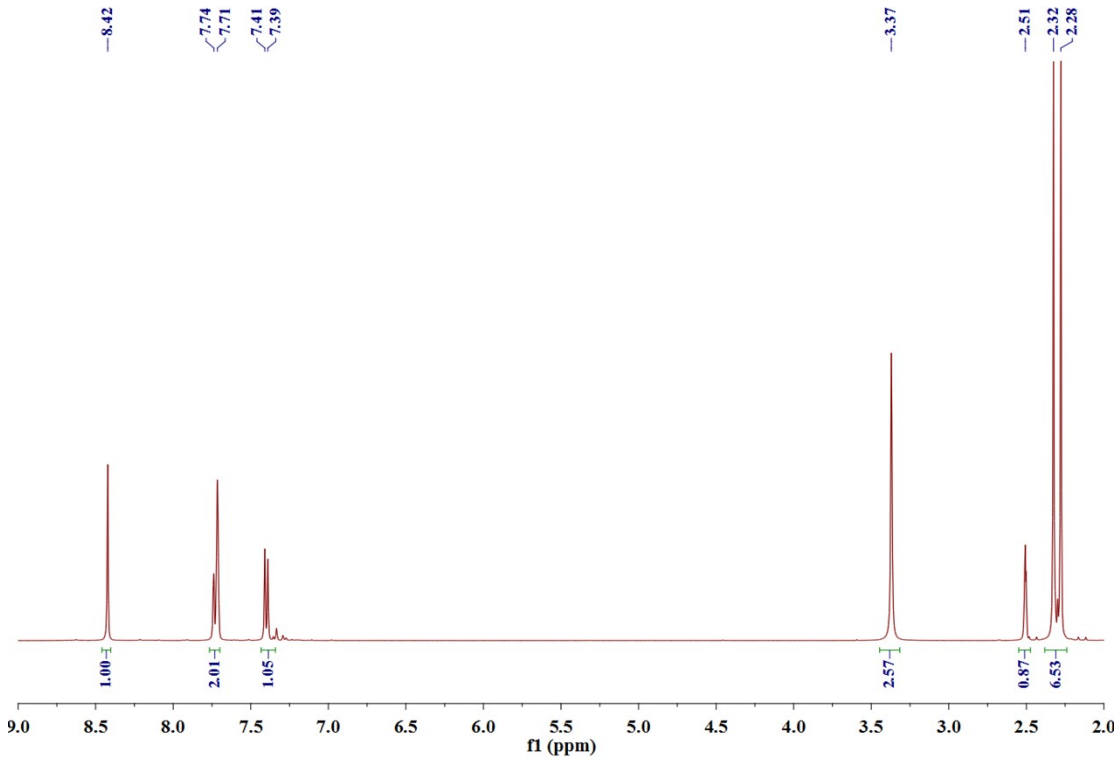

Figure S39. ^{1}H NMR spectrum of 2-[(3,4-dimethylphenyl)methylidene]propanedinitrile.

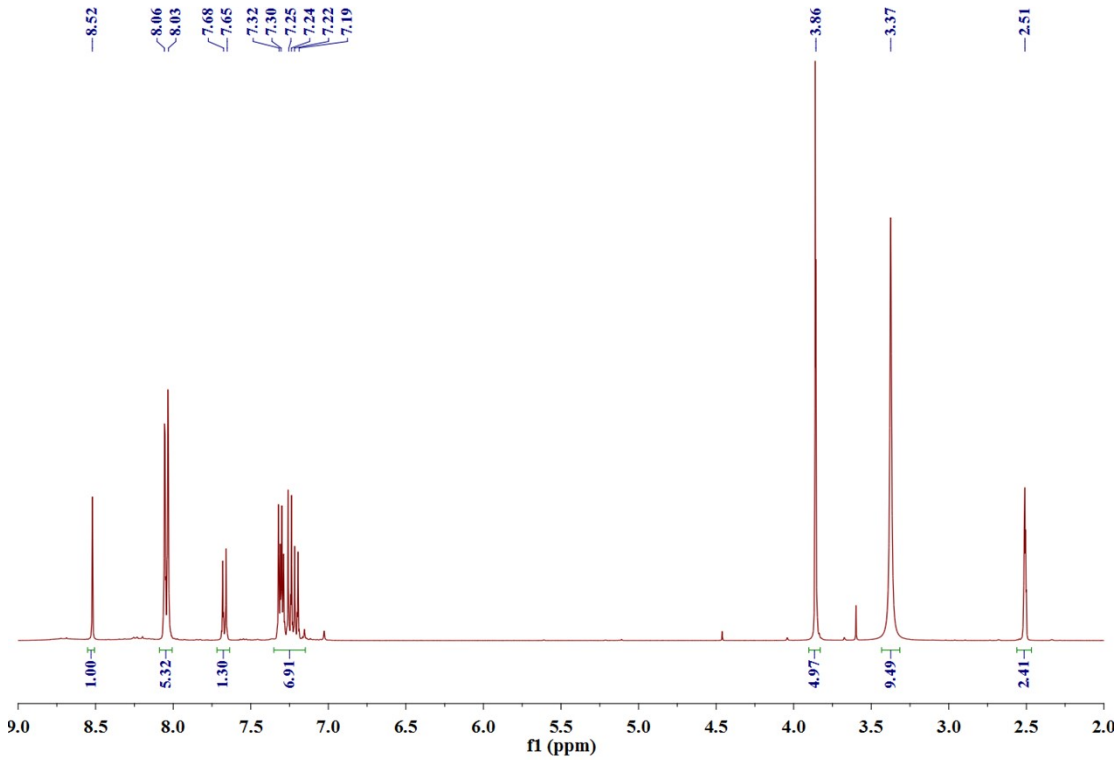

Figure S40. ^{1}H NMR spectrum of methyl 4-[4-(2,2-dicyanoeth-1-en-1-yl)phenoxy]benzoate.

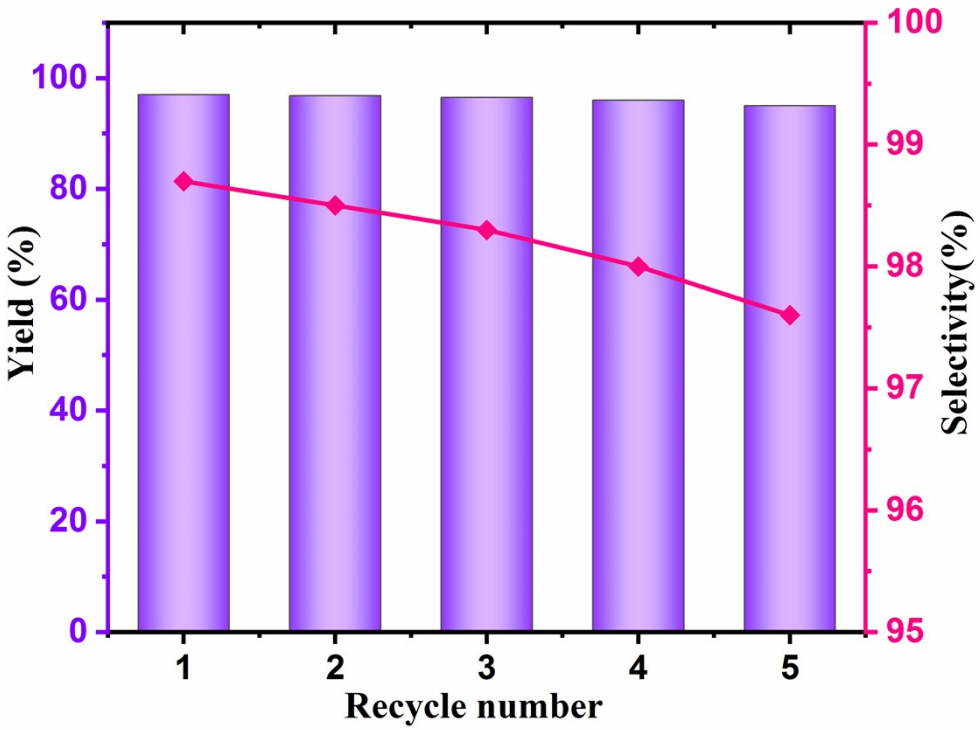

Figure S41. Recyclability study (five cycles) for catalytic activities of **NUC-62** in knoevenagel condensation reaction.

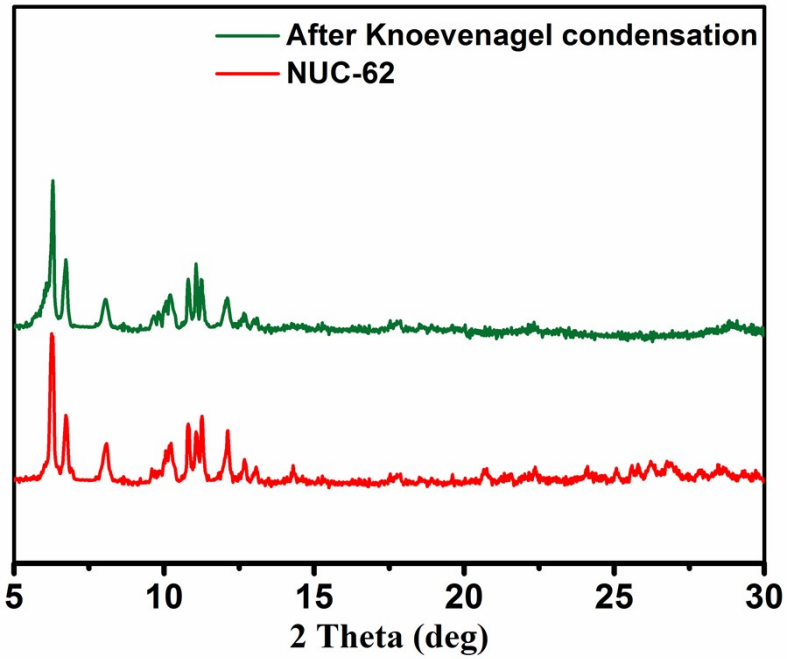

Figure S42. The PXRD patterns of **NUC-62** and used **NUC-62** after fifth knoevenagel condensation reaction.

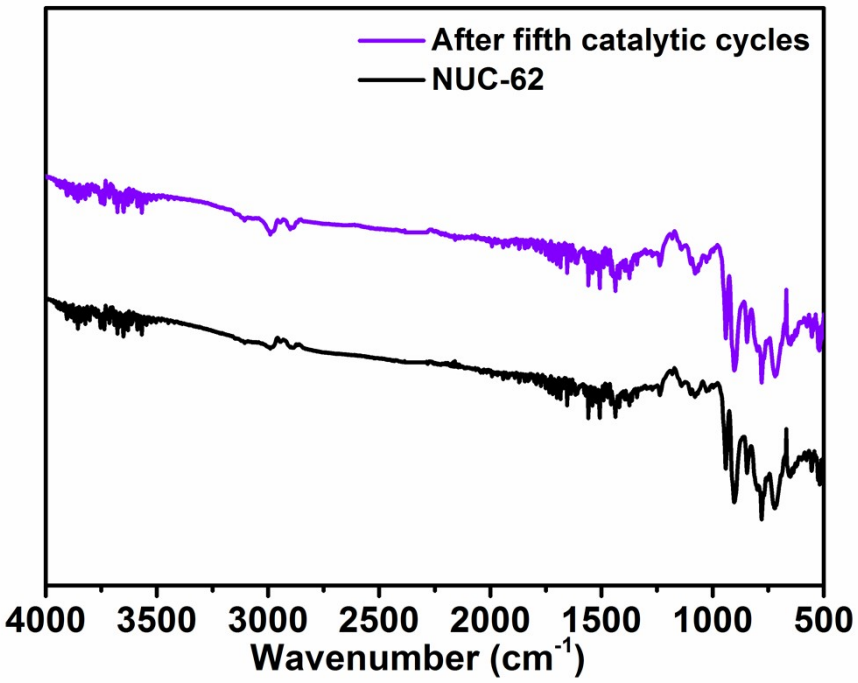

Figure S43. The FT-IR patterns of **NUC-62** and used **NUC-62** after fifth knoevenagel condensation reaction.

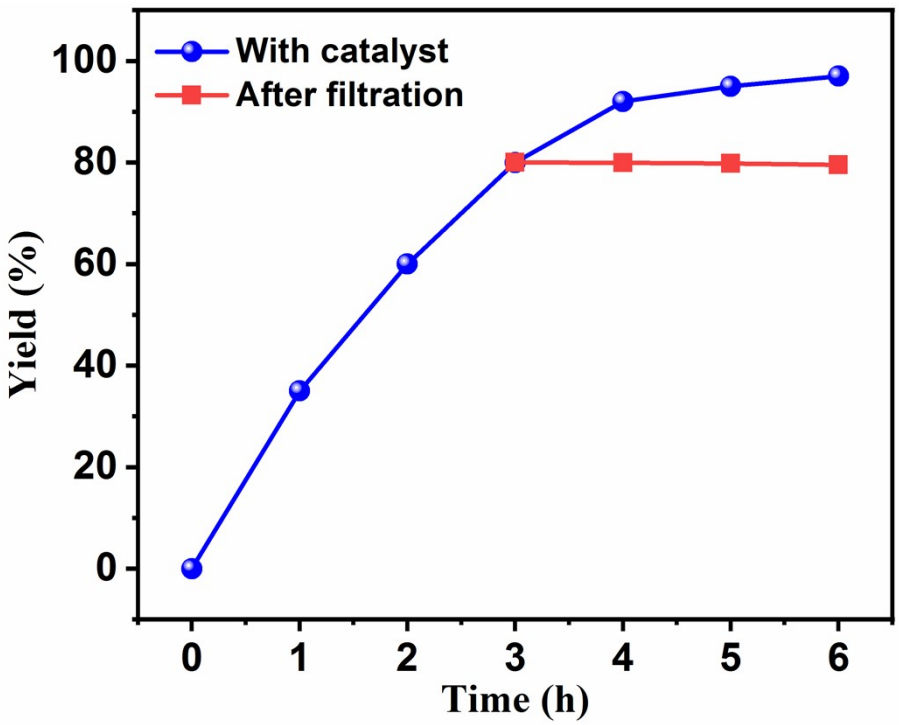

Figure S44. Evidence of heterogeneous nature of **NUC-62** in the knoevenagel condensation reaction.